J. Fluid Mech. (2007), *vol.* 590, *pp.* 117–146.
doi:10.1017/S0022112007008002 Printed in the United Kingdom

Inertial-range intermittency and accuracy of direct numerical simulation for turbulence and passive scalar turbulence

TAKESHI WATANABE[1,2] AND TOSHIYUKI GOTOH[1,2]

[1]Graduate School of Engineering, Department of Engineering Physics, Nagoya Institute of Technology, Gokiso, Showa-ku, Nagoya, 466-8555, Japan

[2]CREST, Japan Science and Technology Agency, 4-1-8 Honcho, Kawaguchi, Saitama 332-0012, Japan

(Received 9 August 2006 and in revised form 19 June 2007)

We examine the effects of the variation in dissipation-range resolution on the accuracy of inertial-range statistics and intermittency in terms of the direct numerical simulations of homogeneous turbulence and passive-scalar turbulence by changing the spatial resolution up to 2048^3 grid points while maintaining a constant Reynolds number at $R_\lambda \simeq 180$ or $\simeq 420$ and Schmidt number at $Sc = 1$. Although large fluctuations of the derivative fields depended strongly on $K_{max}\overline{\eta}$ and were underestimated when $K_{max}\overline{\eta} \simeq 1$, where K_{max} is the maximum wavenumber in the computations and $\overline{\eta}$ is the mean Kolmogorov length, the behaviour of the spectra and the scaling exponents of the structure functions up to the eighth order in the range of scales greater than $10\overline{\eta}$ was insensitive to variations in $K_{max}\overline{\eta}$, even when $K_{max}\overline{\eta} \simeq 1$. The relationship between the spatial resolution and asymptotic tail of the probability density functions of the energy dissipation fields was studied using the multifractal model for dissipation, and the results were confirmed by comparison to the simulation data. Degradation of the statistics arises from modifications to the flow dynamics due to the finite wavenumber cutoff and the use of a coarser filter width for the data, which is obtained using a reasonable accuracy criterion for the flow dynamics. The effect of the former was less than that of the latter for the low-to-moderate-order statistics when $K_{max}\overline{\eta} \geqslant 1$. We also discuss the universality of the inertial-range statistics with respect to variations in the dissipation-range characteristics.

1. Introduction

Recent increases in the power of high-performance computers have been very dramatic and have enabled us to examine more complicated phenomena, such as turbulence, accompanied by wider dynamic scale ranges and multiple physical processes. Direct numerical simulation (DNS) is becoming a very powerful tool to investigate the various dynamical and statistical aspects of turbulence (Pope 2000). Once the turbulent flow field has been obtained numerically, various types of data that are sometimes difficult to access experimentally are easily computed and can provide very useful and important knowledge about the turbulence dynamics and statistics. The detailed images obtained from DNS stimulate us and provide new insight into turbulent flow fields, although these images should be interpreted with caution.

The accuracy of DNS is important in the analysis of turbulence and has been discussed since these simulations were first performed. A prevailing criterion for the

numerical accuracy of DNS is that the smallest scales of the turbulent motion must be adequately resolved on the grid. The size of these scales is conventionally estimated in terms of the mean Kolmogorov length,

$$\overline{\eta} = \left(\frac{\nu^3}{\overline{\epsilon}}\right)^{1/4}, \tag{1.1}$$

where ν is the kinetic viscosity and $\overline{\epsilon}$ is the average rate of energy dissipation per unit mass. If the velocity field is expanded using a Fourier series by assuming periodic boundary conditions in the three directions, which is a common procedure in the DNS of homogeneous turbulence, the above accuracy requirement may be expressed as $\overline{\eta}/\Delta x \sim K_{max}\overline{\eta} > 1$, where $K_{max} \sim 1/\Delta x$ is the maximum wavenumber of the truncation of the Fourier series expansion. In many DNS of homogeneous isotropic turbulence, $K_{max}\overline{\eta} = 1$–$2$ is chosen for physical and economical reasons (Wang, Chen & Brasseur 1999; Yeung, Xu & Sreenivasan 2002; Gotoh, Fukayama & Nakano 2002; Kaneda *et al.* 2003; Yeung, Donzis & Sreenivasan 2005).

The Kolmogorov dissipation length is derived from dimensional arguments. It is useful to define the local Kolmogorov length $\eta(\boldsymbol{x}, t) = (\nu^3/\epsilon(\boldsymbol{x}, t))^{1/4}$ by replacing $\overline{\epsilon}$ of (1.1) with the local value of $\epsilon(\boldsymbol{x}, t) = (\nu/2)(\partial_i u_j + \partial_j u_i)^2$. This means that large fluctuations in $\epsilon(\boldsymbol{x}, t)$ lead to small $\eta(\boldsymbol{x}, t)$ and that regions exist in which the velocity field is under-resolved because $\eta(\boldsymbol{x}, t)$ fluctuates around $\overline{\eta}$. Sreenivasan (2004) and Yakhot & Sreenivasan (2005) pointed out that the conventional criterion for the resolution of the mean Kolmogorov length is inaccurate and the strong intermittency in the energy dissipation poses a more stringent resolution requirement for DNS than $K_{max}\overline{\eta} = 1$–$2$.

The most stringent condition for resolving the smallest Kolmogorov scale is

$$K_{max}\eta_{min} > 1, \tag{1.2}$$

where η_{min} is the smallest dissipation scale defined by

$$\eta_{min} = \left(\frac{\nu^3}{\epsilon_{max}}\right)^{1/4} = \left(\frac{\epsilon_{max}}{\overline{\epsilon}}\right)^{-1/4} \overline{\eta} \tag{1.3}$$

and ϵ_{max} is the largest value of $\epsilon(\boldsymbol{x})$. If we apply multifractal theory to the energy dissipation intermittency (see the Appendix or Meneveau & Sreenivasan 1991), ϵ_{max} can be evaluated using

$$\frac{\epsilon_{max}}{\overline{\epsilon}} \sim R_\lambda^{6(1-\alpha_{min})/(3+\alpha_{min})}, \tag{1.4}$$

where R_λ is the Taylor-microscale Reynolds number and α is the local singularity exponent defined by $\epsilon_r \sim \overline{\epsilon}(r/L)^{\alpha-1}$ (see (A 6) in the Appendix) (Meneveau & Sreenivasan 1991; Frisch 1995). The exponent α_{min} represents the minimum value in the distribution of α, which based on experiments is approximately $\alpha_{min} \simeq 0.3$ (Meneveau & Sreenivasan 1991), while the Kolmogorov theory (Kolmogorov 1941) yields the constant value of $\alpha = 1$. The most intermittent case is given by $\alpha_{min} = 0$ and $\eta_{min} \sim R_\lambda^{-1/2}\overline{\eta} \ll \overline{\eta}$ when $R_\lambda \gg 1$, so that $K_{max}\eta_{min} \sim R_\lambda^{-1/2}K_{max}\overline{\eta} > 1$ requires $K_{max}\overline{\eta} > R_\lambda^{1/2}$, a very severe limitation. It is reasonable to assume that any physical quantities that have spectral support near the dissipation-wavenumber range are contaminated by insufficient resolution and that even the inertial-range statistics suffer from under-resolution effects in the dissipation range.

Although similar arguments can be applied to a passive scalar convected by turbulence, the DNS accuracy requirements are more stringent. The mean Batchelor

length $\overline{\eta}_B = (\kappa^2\nu/\overline{\epsilon})^{1/4}$ varies with the Schmidt number $Sc = \nu/\kappa$, where κ is the scalar diffusivity, which is related to the mean Kolmogorov length $\overline{\eta}$ as

$$\overline{\eta}_B = Sc^{-1/2}\overline{\eta}. \tag{1.5}$$

When the Schmidt number is greater than unity, a reasonable DNS resolution criterion for the scalar field becomes much harder to satisfy. Even for the case of $Sc = 1$, i.e. $\overline{\eta} = \overline{\eta}_B$, a passive-scalar DNS should satisfy the stronger condition $K_{max}\overline{\eta} \geqslant 1.4$ rather than $K_{max}\overline{\eta} = 1$ (Wang *et al.* 1999; Yeung *et al.* 2002, 2005). Wang *et al.* (1999) have shown that the scaled peak wavenumber $k_p^\theta\overline{\eta} = 0.25$ of the dissipation spectrum for the scalar variance is greater than that for the kinetic energy, $k_p\overline{\eta} \simeq 0.16$; the ratio is $k_p^\theta/k_p = 1.4$. This is due to the efficient transfer of the scalar variance and the more non-local nature of the triad interaction (Gotoh & Watanabe 2005). The scalar dissipation field for the scalar variance, defined by $\chi(\boldsymbol{x}) = \kappa(\partial_i\theta)^2$, also fluctuates more intermittently than the energy dissipation, and its intermittency effects on the accuracy of the DNS are more substantial (Chen & Cao 1997; Mydlarski & Warhaft 1998; Warhaft 2000; Shraiman & Siggia 2000).

Schumacher, Sreenivasan & Yeung (2005) have investigated the very fine structures and statistics of the scalar dissipation field χ (ϵ_θ in their paper). For $R_\lambda = 10$ and 24, and $Sc = 2$, 8, and 32, they examined the effects of the spatial resolution of the scalar field on the statistics by changing the spatial resolution from $K_{max}\overline{\eta} \approx 8.4$ to 33.6. The probability density function (PDF) of χ from a lower-resolution DNS slightly underestimated the PDF curve from a finer-resolution DNS at both small and large amplitudes, although the two PDF curves collapsed at medium amplitudes. The generalized dimension D_q at negative q of χ from the lower-resolution DNS was less than that of the finer-resolution DNS, indicating that the calm region was affected more by the lower resolution. Since the asymptotic tail of the PDF is linked to any sharpening of the PDF peak through normalization, it is quite plausible that poor resolution affected the peak of the PDF as well as the tail. They also suggested that the most intense scalar dissipation does not necessarily occur in the very fine scalar dissipation structures.

The study of Schumacher *et al.* (2005) was made at low Reynolds numbers and the Schmidt number $Sc = 2$–32, where the dissipation fields of the energy and scalar variance were well resolved, but no inertial or inertial convective ranges were established. In many cases, recent high-resolution DNS have been performed to investigate the dynamical and statistical laws of (scalar) turbulence in the inertial and inertial convective ranges at very high Reynolds numbers. To achieve a Reynolds number that is as high as possible and a scaling range that is as wide as possible, most DNS have been (and will be) performed using the resolution condition of $K_{max}\overline{\eta} \approx 1$. If under-resolution in the (scalar) dissipation range affects the statistics and dynamics in the inertial (or larger scale) range, it is critical to know to what extent the turbulent dynamics are sensitive to the variation in $K_{max}\overline{\eta}$, or what statistics of velocity and scalar fields are sensitive or insensitive to the effects of the dissipation intermittency. Before engaging in further high-resolution DNS research, we should determine the extent to which the value of $K_{max}\overline{\eta}$ is minimized in a DNS with a reasonable degree of accuracy (Gotoh *et al.* 2002; Kaneda *et al.* 2003). To our knowledge, no comprehensive studies have examined the energy and scalar dissipation intermittency effects on the accuracy of DNS with a special emphasis on the statistics in the inertial and inertial convective ranges.

We performed two series of DNS at $R_\lambda = 180$ and 420 by varying only the grid spacing Δx (or the maximum wavenumber K_{max}) while leaving the other conditions

unchanged, and examined changes in the resulting statistical behaviour. This is similar to the study of Schumacher *et al.* (2005) but with a special focus on the scaling properties of the velocity and scalar fields in the inertial-range scale. We quantitatively examined how the variation of $\Delta x/\overline{\eta}$ ($K_{max}\overline{\eta}$) affected the behaviour of statistics in scales larger and smaller than $\overline{\eta}$.

This paper is organized as follows. Section 2 describes the DNS performed in the present study. Section 3 presents the results of a statistical analysis of the DNS data, where the $K_{max}\overline{\eta}$ dependences of the derivative statistics (§ 3.1), behaviour of the spectra and transfer fluxes (§ 3.2), scaling properties of the structure functions at lower orders (§ 3.3) and higher orders (§ 3.4), and the variations in the velocity and scalar-increment PDFs (§ 3.5) are examined in detail. Section 4 examines the relationship between the asymptotic tails of the dissipation PDFs and the spatial resolution. The origin of the statistical degradation is studied. The implications of the present results regarding the variation of $K_{max}\overline{\eta}$ are also discussed. We summarize the results and give our conclusions in § 5.

2. Direct numerical simulations

The incompressible velocity field $u_i(\boldsymbol{x}, t)(i = 1, 2, 3)$ and the scalar field $\theta(\boldsymbol{x}, t)$ are assumed to be governed by the Navier–Stokes and advection–diffusion equations,

$$(\partial_t + u_j\partial_j)u_i = -\partial_i P + \nu\partial_j^2 u_i + f_i, \quad \partial_i u_i = 0, \tag{2.1a,b}$$

$$(\partial_t + u_j\partial_j)\theta = \kappa\partial_j^2\theta + f_\theta, \tag{2.2}$$

respectively. We considered only the case with a Schmidt number $Sc = 1$ throughout this paper so that there were equal contributions from the molecular action to the small-scale nature of the velocity and scalar fields. The terms f_i and f_θ are the external solenoidal Gaussian random force and scalar sources, respectively. They had spectral support in the low-wavenumber band $1 \leqslant |\boldsymbol{k}| \leqslant 2$ to maintain a statistical steady state (see Gotoh *et al.* 2002; Watanabe & Gotoh 2004). Equations (2.1*a*, *b*) and (2.2) were numerically integrated in a periodic box of size $\mathscr{L} = 2\pi$. A pseudospectral method was used for the nonlinear and convective terms, and the time integration was performed using a fourth-order Runge–Kutta–Gill method.

In the present study, the two series of DNS were characterized by two Taylor-microscale Reynolds numbers. For each Reynolds number, the grid size $\Delta x = 2\pi/N$ (or maximum wavenumber $K_{max} = \sqrt{2}N/3$) was the only control parameter. N is the number of grid points in one direction. The DNS parameters and the time-averaged fundamental statistics are summarized in table 1. The series of lower R_λ (referred to as series L runs) consisted of runs L1 ($N = 256$, $K_{max}\overline{\eta} = 1.0$), L2 ($N = 512$, $K_{max}\overline{\eta} = 2.0$), and L3 ($N = 1024$, $K_{max}\overline{\eta} = 3.8$). The series of higher R_λ (referred to as series H runs) consisted of runs H1 ($N = 1024$, $K_{max}\overline{\eta} = 1.1$) and H2 ($N = 2048$, $K_{max}\overline{\eta} = 2.2$). We obtained turbulent states with $R_\lambda \simeq 180$ for the series L runs and $R_\lambda \simeq 420$ for the series H runs, irrespective of N. A portion of the results for the series L runs has already been discussed in a previous study (Watanabe & Gotoh 2006*a*), and the detailed results for run H1 can be found in Watanabe & Gotoh (2004). The kinetic energy and scalar variance are defined by

$$E = \frac{1}{2}\langle u_i^2\rangle = \int_0^\infty E(k)\,\mathrm{d}k, \quad E_\theta = \frac{1}{2}\langle\theta^2\rangle = \int_0^\infty E_\theta(k)\,\mathrm{d}k, \tag{2.3a,b}$$

Run	L1	L2	L3	H1	H2
N^3	256^3	512^3	1024^3	1024^3	2048^3
R_λ $(= P_\lambda)$	176 ± 17	178 ± 10	180 ± 8	427 ± 10	414
ν $(= \kappa)$	1.3×10^{-3}	1.3×10^{-3}	1.3×10^{-3}	2.4×10^{-4}	2.4×10^{-4}
$\overline{\eta}(\times 10^{-3})$	8.3 ± 0.3	8.2 ± 0.2	7.8 ± 0.2	2.20 ± 0.03	2.27
$K_{max}\overline{\eta}$	1.0	2.0	3.8	1.1	2.2
T_{av}	21.16	4.35	3.61	2.43	—
E	1.68 ± 0.17	1.76 ± 0.07	1.94 ± 0.09	1.97 ± 0.09	1.79
$\overline{\epsilon}$	0.468 ± 0.066	0.501 ± 0.040	0.593 ± 0.046	0.591 ± 0.030	0.519
$\hat{\epsilon}$	0.477 ± 0.056	0.472 ± 0.034	0.496 ± 0.034	0.464 ± 0.008	0.466
$-S_u$	0.507 ± 0.006	0.542 ± 0.004	0.555 ± 0.014	0.558 ± 0.004	0.599
λ	0.217 ± 0.015	0.214 ± 0.010	0.206 ± 0.007	0.0895 ± 0.0008	0.0910
L	1.20 ± 0.08	1.19 ± 0.05	1.23 ± 0.07	1.18 ± 0.03	1.17
E_θ	0.88 ± 0.13	0.85 ± 0.11	0.78 ± 0.11	0.99 ± 0.11	0.71
$\overline{\chi}$	0.502 ± 0.082	0.485 ± 0.066	0.456 ± 0.049	0.598 ± 0.038	0.493
$\hat{\chi}$	0.324 ± 0.042	0.319 ± 0.043	0.321 ± 0.040	0.315 ± 0.035	0.370
$-S_{u\theta}$	0.430 ± 0.014	0.520 ± 0.005	0.515 ± 0.018	0.443 ± 0.005	0.507
λ_θ	0.118 ± 0.008	0.117 ± 0.006	0.115 ± 0.008	0.0488 ± 0.0024	0.0457
L_θ	0.770 ± 0.079	0.777 ± 0.072	0.781 ± 0.099	0.826 ± 0.073	0.657

TABLE 1. DNS parameters.

where $E(k)$ and $E_\theta(k)$ are the spectra for the kinetic energy and scalar variance, respectively. The angle brackets $\langle \cdots \rangle$ indicate the spatial and temporal averages. The duration of the temporal average was T_{av}, which is the integration time normalized by the large-eddy turnover time $T_{eddy} = L/\sqrt{2E/3}$ during steady state. The mean dissipation rates for E and E_θ are

$$\overline{\epsilon} = \frac{\nu}{2}\langle(\partial_i u_j + \partial_j u_i)^2\rangle, \quad \overline{\chi} = \kappa\langle(\partial_i \theta)^2\rangle, \tag{2.4a,b}$$

and the skewness or mixed skewness of the longitudinal velocity and scalar gradients are defined by

$$S_u = \frac{\langle(\partial_1 u_1)^3\rangle}{\langle(\partial_1 u_1)^2\rangle^{3/2}}, \quad S_{u\theta} = \frac{\langle(\partial_1 u_1)(\partial_1 \theta)^2\rangle}{\langle(\partial_1 u_1)^2\rangle^{1/2}\langle(\partial_1 \theta)^2\rangle}. \tag{2.5a,b}$$

Several characteristic scales, such as the integral scales, $L = (3\pi/4E)\int_0^\infty k^{-1}E(k)\,\mathrm{d}k$ and $L_\theta = (\pi/2E_\theta)\int_0^\infty k^{-1}E_\theta(k)\,\mathrm{d}k$, Taylor microscales, $\lambda = \sqrt{\langle u_1^2\rangle/\langle(\partial_1 u_1)^2\rangle}$ and $\lambda_\theta = \sqrt{\langle\theta^2\rangle/\langle(\partial_1\theta)^2\rangle}$, and the Kolmogorov and Batchelor scales, $\overline{\eta}$ and $\overline{\eta}_B$, were almost identical, irrespective of N, provided that R_λ remained unchanged. The errors given for the averaged quantities in tables 1 and 2 and the error bars shown in figures 2 and 10 were estimated from the standard deviations of the temporal fluctuations in the quantities during the averaging time. In all runs, the normalized mean dissipations $\hat{\epsilon} = \overline{\epsilon}L/u_{rms}^3$ and $\hat{\chi} = \overline{\chi}L/u_{rms}\theta_{rms}^2$, where $u_{rms} = \sqrt{2E/3}$ and $\theta_{rms} = \sqrt{2E_\theta}$, respectively, roughly converged with respect to $K_{max}\overline{\eta}$, although some fluctuations were observed in their values. Deviations in the average values of $\hat{\epsilon}$ and $\hat{\chi}$ in runs L3 and H2 from those of other runs were due to the non-stationary effects in u_{rms} and θ_{rms}, which are quantities dominated by large scales with longer time variations and thus easily affected when the averaged time is short. The statistical data obtained from the finest DNS (run H2) was evaluated by analysing a single snapshot of the velocity and scalar fields because of the limited amount of available computational time. Therefore, we

could not evaluate errors due to the temporal average. This implies that the large-scale statistics were poorly converged compared to run H1 and that we must exercise caution when analysing them.

3. Results

3.1. *Effects on the derivative statistics*

It is reasonable to assume that the statistics of the velocity and scalar gradients are sensitive to variations in the grid size Δx. The finiteness of the spatial resolution manifests itself during the post-processing to compute the derivative field from the raw field data, such as the dependence on the order of the finite difference method, even when the equation of motion is adequately integrated, and in modifications to the actual turbulence dynamics or the dynamics of the attractor of the equation of motion by limiting the functional space. Since the differentiation in the present study was performed using inverse Fourier transformations, e.g. $\partial_1\theta = \sum_{\boldsymbol{k}} \mathrm{i}k_1\theta(\boldsymbol{k})\exp(\mathrm{i}\boldsymbol{k}\cdot\boldsymbol{x})$, the numerical error was minimized. The DNS of the turbulence in terms of the spectral method was therefore adequate to address the second issue. Since the spatial resolution limit is given by a number, K_{max}, it is easy to control the accuracy of the DNS. Changing K_{max} affects the variation in the degrees of freedom contributing to the dynamics, especially to the dissipation, and thus strongly influences the details of the attractor contributing to the strong intermittency. We first quantitatively examined the resolution effects on the behaviour of the one-point PDFs and the normalized moments for several derivative fields. The effects on the modification of the dynamics will be discussed in more detail in § 4.2.

Figure 1 compares normalized PDFs for the longitudinal velocity gradient $\partial_1 u_1$ (denoted by L), transverse velocity gradient $\partial_2 u_1$ (T), and scalar gradient $\partial_1\theta$ (θ) obtained for all runs. The probabilities in their asymptotic tails increased with increase of $K_{max}\overline{\eta}$. To examine this behaviour quantitatively, the variation of the normalized moments $M_{2q} = \langle z^{2q}\rangle/\langle z^2\rangle^q$ with the order of q for the series L runs is shown in figures 2(a) ($z = \partial_1 u_1$) and 2(b) ($z = \partial_1\theta$). The $K_{max}\overline{\eta}$ dependence of M_{2q} became more significant as q increased, which corresponded to the sensitivity of rare events to the variation of $K_{max}\overline{\eta}$, as shown in figure 1. A comparison of the normalized fourth-order moments (flatness) $M_4 = F_\alpha$ (where α denotes labels L, T, and θ) obtained for the series L runs is summarized in table 2. The values from runs L1 and L2 were underestimated compared to those of run L3. Similar trends were also observed for the series H runs. To investigate the resolution effects on small amplitudes of the fluctuations, the central parts of the curves in figures 1(a) and 1(c) were magnified and plotted on a linear scale in figure 1(d). The $\partial_1\theta$ curve for run L1 was considerably lower than the $\partial_1\theta$ curves for runs L2 and L3, which is in sharp contrast to the small differences among the curves for $\partial_1 u_1$. This observation implies that both strong and weak fluctuations of the scalar gradient field are more sensitive to variations in $K_{max}\overline{\eta}$, unlike the velocity gradient field, and thus the resolution effects are more significant in the scalar dissipation, as described by Schumacher *et al.* (2005).

Next, we investigated the PDFs for the dissipation fields $\epsilon(\boldsymbol{x})$ and $\chi(\boldsymbol{x})$. Figure 3 shows the behaviour of the PDFs for $\epsilon/\overline{\epsilon}$ and $\chi/\overline{\chi}$ from the series L runs. The probabilities of rare events increased with increase of $K_{max}\overline{\eta}$. From the finest-resolution DNS (run L3), we roughly estimated $\epsilon_{max}/\overline{\epsilon} \sim 300$, and found that $\eta_{min} \sim \overline{\eta}/4$, i.e. $K_{max}\eta_{min} \simeq 1$ at $R_\lambda = 180$. Therefore, the condition for run L3 approximately satisfied the most stringent DNS resolution requirement, as discussed by Sreenivasan (2004). Figure 3 also indicates that $\chi/\overline{\chi}$ is more intermittent than $\epsilon/\overline{\epsilon}$ because the

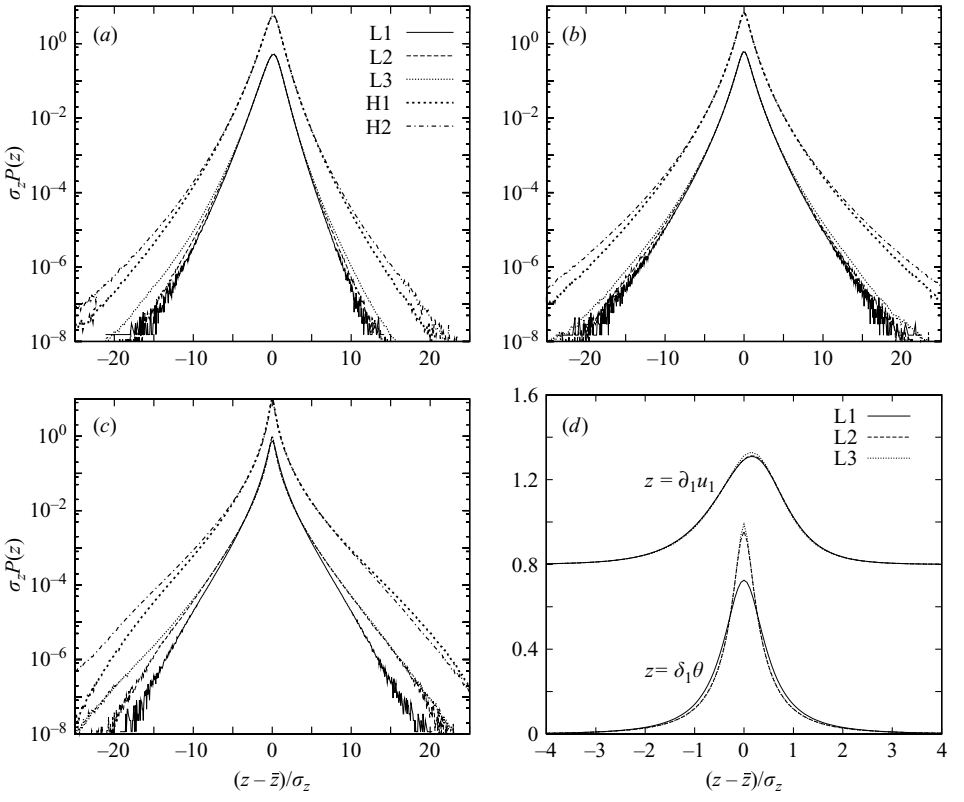

FIGURE 1. $K_{max}\overline{\eta}$ dependences of the one-point PDFs for the (a) longitudinal velocity gradient $\partial_1 u_1$, (b) transverse velocity gradient $\partial_2 u_1$, (c) scalar gradient $\partial_1 \theta$, and (d) magnification of the PDFs at small amplitudes of the fluctuations $\partial_1 u_1$ and $\partial_1 \theta$ for the series L runs. The curves for runs H1 and H2 in (a–c) are multiplied by a factor of 10 for clarity, and the curves for $\partial_1 u_1$ in (d) are shifted by adding a factor of 0.8 to their original values. Note that the curve near the end of tail of PDF for both series runs in (a–c) moves upward as the resolution increases.

	F_L	F_T	F_θ	$\langle(\epsilon/\overline{\epsilon})^2\rangle$	$\langle(\chi/\overline{\chi})^2\rangle$	$\langle(\epsilon/\overline{\epsilon})^3\rangle$	$\langle(\chi/\overline{\chi})^3\rangle$
Run L1	5.72 ± 0.09	8.39 ± 0.11	11.2 ± 0.4	2.66 ± 0.04	6.24 ± 0.22	16.5 ± 1.0	110 ± 16
Run L2	5.99 ± 0.05	8.90 ± 0.13	15.3 ± 0.7	2.80 ± 0.03	8.28 ± 0.35	20.0 ± 0.5	204 ± 20
Run L3	6.61 ± 0.18	9.67 ± 0.30	16.1 ± 0.3	3.05 ± 0.08	8.75 ± 0.18	26.6 ± 2.1	243 ± 13

TABLE 2. Flatness factors for $\partial_1 u_1$ (L), $\partial_2 u_1$ (T), and $\partial_1 \theta$ (θ), and second- and third-order moments for the energy and scalar variance dissipations $\epsilon/\overline{\epsilon}$ and $\chi/\overline{\chi}$. The errors were evaluated from the standard deviation of the temporal fluctuations over T_{av}.

rare fluctuations in $\chi/\overline{\chi}$ had larger probabilities than those of $\epsilon/\overline{\epsilon}$. This feature was also quantitatively confirmed by the moments listed in table 2. The same PDF curves are plotted using a logarithmic scale for both axes in the inset plots of figure 3 to emphasize the resolution effects on the weak fluctuations around their means. The PDFs were almost independent of $K_{max}\overline{\eta}$ over the range of $0.1 < \epsilon/\overline{\epsilon} < 10$ and $0.1 < \chi/\overline{\chi} < 10$. However, the weak intensity of the fluctuations,

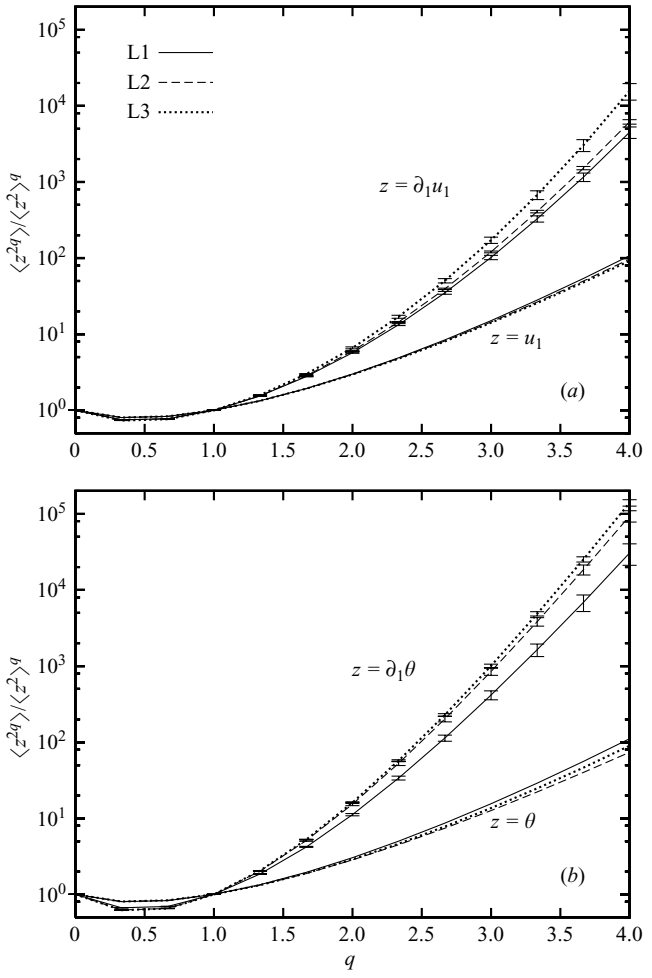

FIGURE 2. $K_{max}\overline{\eta}$ dependences of the normalized moments $M_{2q} = \langle z^{2q}\rangle/\langle z^2\rangle^q$ from the series L runs ($R_\lambda = 180$) for (a) the longitudinal velocity gradient $\partial_1 u_1$ and (b) scalar gradient $\partial_1\theta$. For comparison, M_{2q} for velocity u_1 and scalar θ are also shown. Error bars were estimated from the standard deviations of the temporal fluctuations in the quantities during the averaging time. Note that the curve for $\partial_1 u_1$ and $\partial_1\theta$ moves upward as the resolution increases.

such as $\epsilon/\overline{\epsilon}$, $\chi/\overline{\chi} < 0.1$, were also under-resolved, as shown previously for $Sc = 32$ and $R_\lambda = 10$ (Schumacher *et al.* 2005).

The results obtained in this section can be summarized as follows. The high-order statistics of derivative fields depend significantly on $K_{max}\overline{\eta}$. Many studies on turbulence statistics have focused on the R_λ dependences of the skewness and flatness factors of the velocity and scalar gradients (Monin & Yaglom 1975; Warhaft 2000). The present results suggest that the high-order statistics of derivative fields obtained using a low-resolution DNS, such as runs L1 or H1, should be analysed with great care because the data are generally underestimated. R_λ in the present DNS was much higher than that used by Schumacher *et al.* (2005), but the resolution effects on the dissipation statistics were similar. Therefore, the resolution effects on the derivatives of the passive scalar are significant not only at midrange R_λ and Sc but also for high R_λ and $Sc = O(1)$.

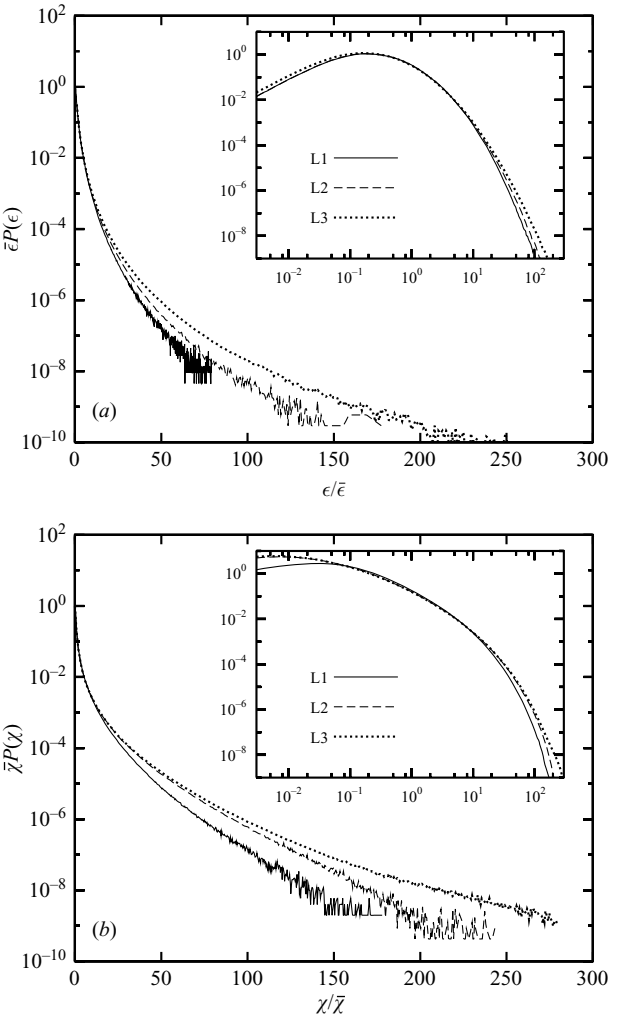

FIGURE 3. $K_{max}\overline{\eta}$ dependences of the PDFs for the (a) kinetic energy dissipation $\epsilon/\bar{\epsilon}$ and (b) scalar variance dissipation $\chi/\bar{\chi}$ from the series L runs. The inset shows the same plots using logarithmic scales for both axes. Note that the curve at the far tail of PDF moves upward as the resolution increases.

3.2. *Effects on the spectral behaviour*

When the Reynolds number is very large, an inertial range (IR) exists in the velocity field and an inertial convective range (ICR) in the scalar field (Kolmogorov 1941; Obukhov 1949; Corrsin 1951). The kinetic energy and scalar variance spectra can be expressed in terms of the Kolmogorov–Obukhov–Corrsin (KOC) theory as

$$E(k) = \bar{\epsilon}^{2/3}k^{-5/3}\hat{E}(k\overline{\eta}), \tag{3.1}$$

$$E_\theta(k) = \overline{\chi}\,\bar{\epsilon}^{-1/3}k^{-5/3}\hat{E}_\theta(k\overline{\eta}_B, Sc), \tag{3.2}$$

where $\hat{E}(x)$ and $\hat{E}_\theta(x, y)$ are non-dimensional functions and it is expected that $\hat{E}(x) = K$ and $\hat{E}_\theta(x, 1) = C_{OC}$ for $x \ll 1$. Note that $\overline{\eta} = \overline{\eta}_B$ because $Sc = 1$. The constants K and C_{OC} are the Kolmogorov and Obukhov–Corrsin constants, respectively. Figure 4 shows $\hat{E}(k\overline{\eta})$ and $\hat{E}_\theta(k\overline{\eta}, 1)$ obtained for all runs. The flat

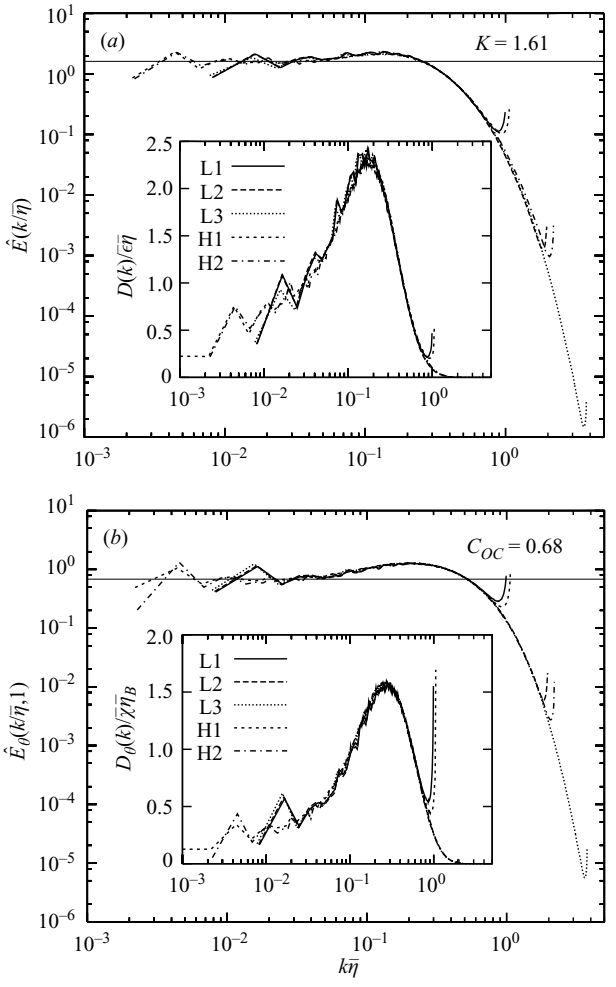

FIGURE 4. Behaviour of the compensated spectra: (*a*) kinetic energy spectrum $\hat{E}(x)$ (3.1) and (*b*) scalar variance spectrum $\hat{E}_\theta(x,1)$ (3.2) from the series L ($R_\lambda = 180$) and H ($R_\lambda = 420$) runs. The horizontal line corresponds to $K = 1.61$ and $C_{OC} = 0.68$, which were evaluated from the results of run H1 (Watanabe & Gotoh 2004). The inset shows the normalized dissipation spectra (3.5*a*, *b*) for both cases.

behaviour is easily seen in the range $0.008 \leqslant k\overline{\eta} \leqslant 0.03$, where the constants were evaluated from run H1 to obtain $K = 1.61$ and $C_{OC} = 0.68$ (Watanabe & Gotoh 2004). The value $K = 1.61$ agrees well with the experimental value 1.62 (Sreenivasan 1995) and the previous DNS value 1.64 (Gotoh *et al.* 2002) though recent DNS and atmospheric observation with higher R_λ than that in the series H runs represent steeper spectra than $k^{-5/3}$ (Kaneda *et al.* 2003; Tsuji 2004). The value $C_{OC} = 0.68$ is consistent with 0.67 which is the value recommended from many experiments (Sreenivasan 1996) and the higher-R_λ passive scalar DNS with a mean scalar gradient (Yeung *et al.* 2005). Except for the range $k \sim K_{max}$, the curves from each series collapsed very well, irrespective of $K_{max}\overline{\eta}$, and those of the series L runs nicely followed the results of the series H runs. These results strongly suggest that the spectra $E(k)$ and $E_\theta(k)$ for wavenumbers below $k\overline{\eta} = 0.8$ were computed accurately, even when the condition $K_{max}\overline{\eta} = 1$ was used for runs L1 and H1.

The spectral equations for the kinetic energy and the scalar variance are expressed as

$$\frac{\mathrm{d}}{\mathrm{d}t}E(k,t) + D(k,t) = T(k,t) + F(k,t), \tag{3.3}$$

$$\frac{\mathrm{d}}{\mathrm{d}t}E_\theta(k,t) + D_\theta(k,t) = T_\theta(k,t) + F_\theta(k,t), \tag{3.4}$$

in terms of the energy and scalar-variance dissipation spectra

$$D(k) = 2\nu k^2 E(k), \quad D_\theta(k) = 2\kappa k^2 E_\theta(k), \tag{3.5a,b}$$

the kinetic-energy transfer function $T(k)$, and the scalar-variance transfer function $T_\theta(k)$ arising from the nonlinear and convective terms in (2.1a,b) and (2.2). The functions $F(k,t)$ and $F_\theta(k,t)$ are spectra of the external injections. The transfer fluxes of the kinetic energy and the scalar variance are defined by

$$\Pi(k) = \int_k^\infty T(k')\,\mathrm{d}k', \quad \Pi_\theta(k) = \int_k^\infty T_\theta(k')\,\mathrm{d}k', \tag{3.6a,b}$$

respectively. The normalized dissipation spectra at various resolutions are plotted in the inset of figure 4 for both R_λ cases. The spectra $D(k)$ and $D_\theta(k)$ around $k \sim K_{max}$ for runs L1 and H1 were significantly affected by the truncation of the Fourier series. In particular, $D_\theta(k)$ was contaminated more than $D(k)$. However, the curves in the range $0.02 \leqslant k\overline{\eta} \leqslant 0.8$, where $D(k)$ and $D_\theta(k)$ contribute to most of the $\overline{\epsilon}$ and $\overline{\chi}$, were insensitive to the variation in $K_{max}\overline{\eta}$ and R_λ. Figure 5 shows the transfer fluxes, for which no significant $K_{max}\overline{\eta}$ dependences were visible across the entire wavenumber range except the integral scales for run H2. These results suggest that the resolution effects on the behaviour of the second- and third-order statistics in wavenumber space were negligible for the entire wavenumber range except $k \sim K_{max}$. Thus, we assume that the accuracy of the passive scalar turbulence in a DNS is satisfactory in the lower-order statistics ranging from the ICR to the dissipation range, even when $K_{max}\overline{\eta} = 1$.

We investigated resolution effects on the spectral behaviour over the dissipation range of $0.5 < k\overline{\eta} < 4$. Several studies have examined the spectral form of the energy and scalar variance over this range (Kerr 1990; Chen *et al.* 1993; Pope 2000; Ishihara *et al.* 2005). The functional forms of $E(k)$ and $E_\theta(k)$ in the dissipation range are

$$E(k) = C(k\overline{\eta})^\alpha \exp(-\beta k\overline{\eta}), \quad E_\theta(k) = C_\theta(k\overline{\eta}_B)^{\alpha_\theta} \exp(-\beta_\theta k\overline{\eta}_B), \tag{3.7a,b}$$

respectively, where C (C_θ), α (α_θ), and β (β_θ) are constants that may depend on R_λ, Sc, and the wavenumber range (e.g. Ishihara *et al.* 2005). To test the form of (3.7a,b) and examine any resolution effects, it is useful to define the local slopes of $E(k)$ and $E_\theta(k)$ by

$$\frac{\mathrm{d}\log E(k)}{\mathrm{d}\log k} = \alpha - \beta(k\overline{\eta}), \quad \frac{\mathrm{d}\log E_\theta(k)}{\mathrm{d}\log k} = \alpha_\theta - \beta_\theta(k\overline{\eta}_B). \tag{3.8a,b}$$

Figure 6 shows the local slopes of $E(k)$ and $E_\theta(k)$ obtained for the series L runs, where the derivative in (3.8a,b) is approximated by the finite difference of $E(k)$ (and $E_\theta(k)$) after smoothing the zigzag curves. As shown in figure 6, we could not observe a significant resolution dependence of the local slopes over the range $0.5 < k\overline{\eta} < 3$. The same trends were also observed for the series H runs (figures not shown). If the functional form of (3.7a,b) is correct, the curves of the local slopes will appear as straight lines according to (3.8a,b). However, figure 6 indicates that the local slopes

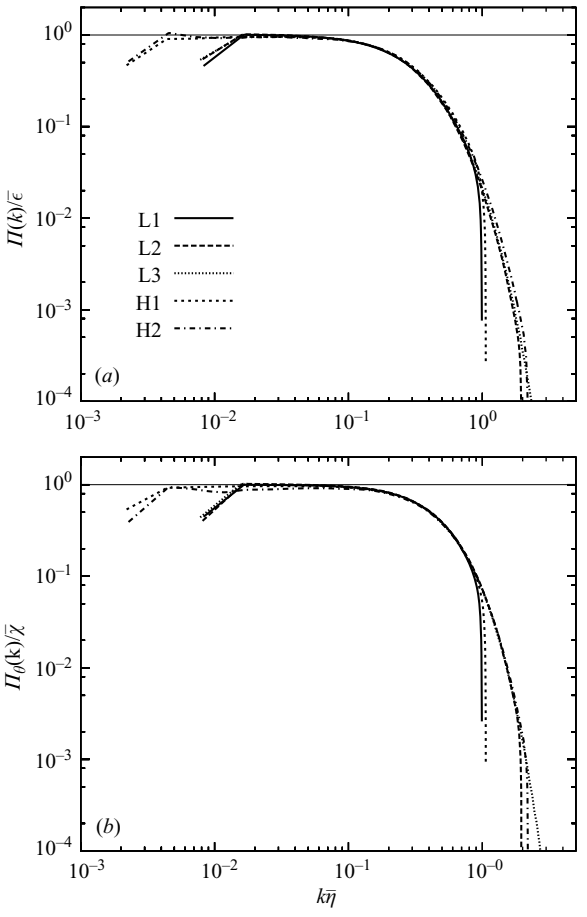

FIGURE 5. $K_{max}\bar{\eta}$ dependences of the normalized transfer fluxes (3.6a,b) for the (a) kinetic energy and (b) scalar variance. The horizontal line corresponds to unity.

for both $E(k)$ and $E_\theta(k)$ bend slightly and cannot be fitted by a single straight line over the range $0.5 < k\bar{\eta} < 3$. If we restrict ourselves to the wavenumber range $0.5 < k\bar{\eta} < 1.5$ for $E(k)$ and $0.2 < k\bar{\eta}_B < 1.5$ for $E_\theta(k)$, we obtain an estimate of $(\alpha, \beta) = (-2.2, 4.1)$ and $(\alpha_\theta, \beta_\theta) = (-0.9, 4.5)$. In the deeper dissipation range of $2 < k\bar{\eta} < 3$, the constants are $(\alpha, \beta) = (-4.3, 2.9)$ and $(\alpha_\theta, \beta_\theta) = (-3.9, 3.1)$.

It is interesting to note that the rate of the exponential decay of $E(k)$ is slightly less than that of $E_\theta(k)$, and that the width of the fitting range for $E_\theta(k)$ is wider than that of $E(k)$. Although the total strain from the wavenumber components below $k_d \sim 1/\bar{\eta}$ is responsible for the average decay of both spectra in the dissipation range, and the local strong fluctuations of the dissipation dominate the decay rate in the far deeper dissipation range because $E(k, \boldsymbol{x}) \propto \exp(-k\tilde{\eta}(\boldsymbol{x}))$ in the subregion of a periodic box with centre $\boldsymbol{x}$ (Kraichnan 1967; Chen *et al.* 1993), it is not clear whether the difference in the decay exponents for the body of the dissipation range survives when $Sc = 1$ and the Reynolds number becomes larger. Detailed discussions of the spectral forms in the dissipation range for several Schmidt and Reynolds numbers can be found in the spectral theory (Batchelor, Howells & Townsend 1959; Kraichnan 1968; Goto & Kida 1999; Gotoh, Nagaki & Kaneda 2000) and DNS (Kerr 1990; Chen *et al.* 1993; Bogucki, Domaradzki & Yeung 1997; Schumacher *et al.* 2005; Ishihara *et al.* 2005)

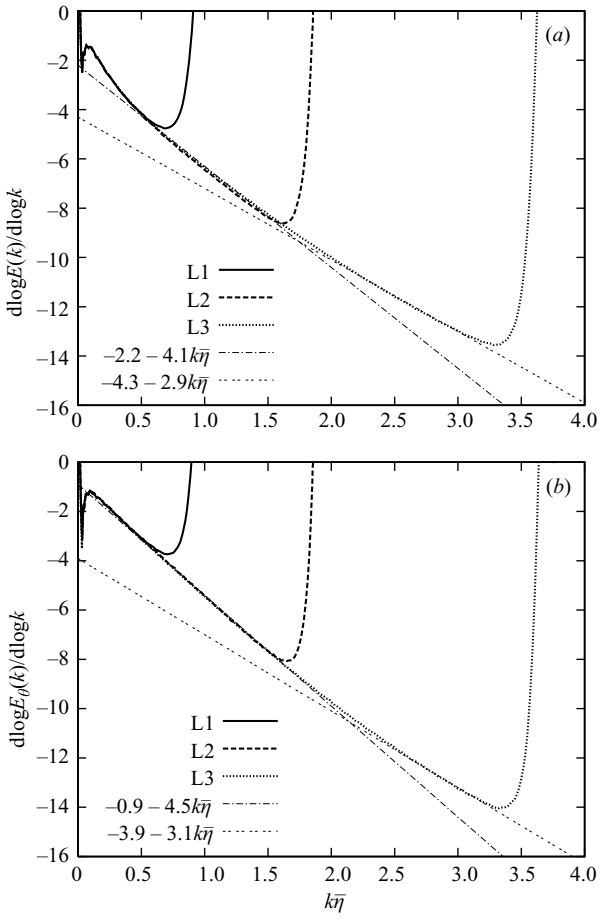

FIGURE 6. Variations in the local slopes of (*a*) $E(k)$ and (*b*) $E_\theta(k)$ against $k\overline{\eta}$ from the series L runs. The functional forms predicted by (3.7*a*, *b*) correspond to the straight lines in each figure, where the parameters (α, β) and $(\alpha_\theta, \beta_\theta)$ are evaluated by curve-fitting over each wavenumber range.

studies. Since the dissipation range width in our DNS was not sufficiently long, we do not discuss this point further.

3.3. *Effects on the second- and third-order structure functions*

The structure functions $S_q^\alpha(r)$ (where α denotes the labels L, T, θ, and θL) for the longitudinal velocity increment δu_r (L), transversal velocity increment δv_r (T), scalar increment $\delta\theta_r$ (θ), and mixed velocity–scalar increment $\delta u_r \delta\theta_r^2$ (θL) are defined as follows:

$$S_q^L(r) = \langle|\delta u_r|^q\rangle, \qquad S_q^T(r) = \langle|\delta v_r|^q\rangle, \tag{3.9a,b}$$

$$S_q^\theta(r) = \langle|\delta\theta_r|^q\rangle, \qquad S_q^{\theta L}(r) = \left\langle\left|\delta u_r \delta\theta_r^2\right|^{q/3}\right\rangle. \tag{3.9c,d}$$

The KOC theory suggests the following scaling forms:

$$S_q^L(r) = (\overline{\epsilon}r)^{q/3}\hat{S}_q^L\left(\frac{r}{\overline{\eta}}, \frac{L}{\overline{\eta}}\right), \qquad S_q^T(r) = (\overline{\epsilon}r)^{q/3}\hat{S}_q^T\left(\frac{r}{\overline{\eta}}, \frac{L}{\overline{\eta}}\right), \tag{3.10a,b}$$

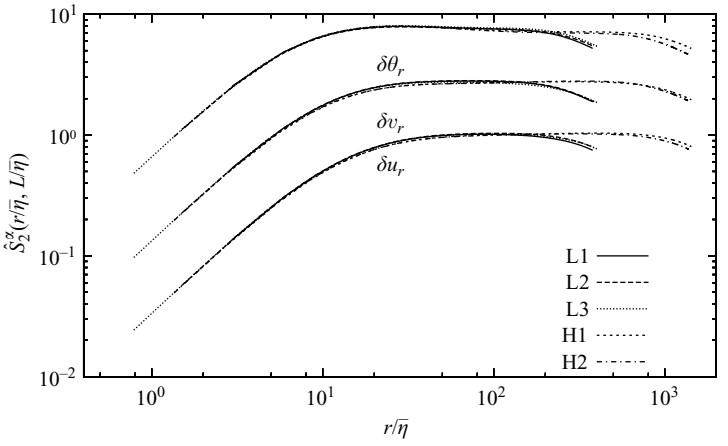

FIGURE 7. $K_{max}\overline{\eta}$ dependences of the compensated second-order structure functions for the longitudinal velocity increment (L), transverse velocity increment (T), and scalar increment (θ). The curves for δu_r (L) and $\delta\theta_r$ (θ) are multiplied by factors of 0.5 and 2, respectively, for clarity.

$$S_q^\theta(r) = (\overline{\chi}^{3/2}\overline{\epsilon}^{-1/2}r)^{q/3}\hat{S}_q^\theta\left(\frac{r}{\overline{\eta}}, \frac{L}{\overline{\eta}}\right), \quad S_q^{\theta L}(r) = (\overline{\chi}r)^{q/3}\hat{S}_q^{\theta L}\left(\frac{r}{\overline{\eta}}, \frac{L}{\overline{\eta}}\right), \quad (3.10c,d)$$

where $\hat{S}_q^\alpha(x, y)$ is a non-dimensional function that is asymptotically $\hat{S}_q^\alpha(x, \infty) =$ constant for $x \gg 1$ if the KOC theory is correct. The compensated second-order structure functions $\hat{S}_2^\alpha$ are shown in figure 7. In contrast to the rise in the spectra near $k\overline{\eta} = 1$ for runs L1 and H1, as shown in figure 4, no significant $K_{max}\overline{\eta}$ dependence of $\hat{S}_2^\alpha$ was observed over the entire range. At $r/\overline{\eta} = 2 \sim 5$, the slope of every curve was approximately 4/3, which implies that $S_2^\alpha(r) \propto r^2$ for very small r. A small deviation in run L3 and H2 curves from the others observed for $r > L$ arose because a statistical convergence was not sufficiently established at this scale due to an insufficient time average.

Next, we examined the resolution effects on the third-order structure functions. The structure function equations can be derived exactly from the fundamental equations of motion (2.1a,b) and (2.2) by assuming statistical isotropy and homogeneity as follows:

$$\langle \delta u_r^3 \rangle = -\frac{4}{5}\overline{\epsilon}r + 6\nu\frac{\mathrm{d}}{\mathrm{d}r}\langle \delta u_r^2 \rangle + F(r), \quad (3.11)$$

$$\langle \delta u_r \delta\theta_r^2 \rangle = -\frac{4}{3}\overline{\chi}r + 2\kappa\frac{\mathrm{d}}{\mathrm{d}r}\langle \delta\theta_r^2 \rangle + F_\theta(r), \quad (3.12)$$

where $F(r)$ and $F_\theta(r)$ are derived from the external force or injection, respectively. In the scale ranges $\overline{\eta} \ll r \ll L$ for (3.11) and $\overline{\eta}_B \ll r \ll L$ for (3.12), the second and third terms on the right-hand sides are much less than the first term. Thus, (3.11) and (3.12) yield asymptotically exact statistical laws, the so-called 4/5 and 4/3 laws: $\langle \delta u_r^3 \rangle = -(4/5)\overline{\epsilon}r$ and $\langle \delta u_r \delta\theta_r^2 \rangle = -(4/3)\overline{\chi}r$, respectively (Yaglom 1949; Monin & Yaglom 1975). Figure 8 shows the variations in $-\langle \delta u_r^3 \rangle/\overline{\epsilon}r$ and $-\langle \delta u_r \delta\theta_r^2 \rangle/\overline{\chi}r$ with $r/\overline{\eta}$ obtained from the present DNS. The plateaux of the compensated 4/5 and 4/3 laws obtained from the series L runs are narrower than those obtained from the series H runs because of the lower R_λ. The curves for all runs were again almost independent of $K_{max}\overline{\eta}$, except over range $r > L$. The difference of curves over the range of $r > L$

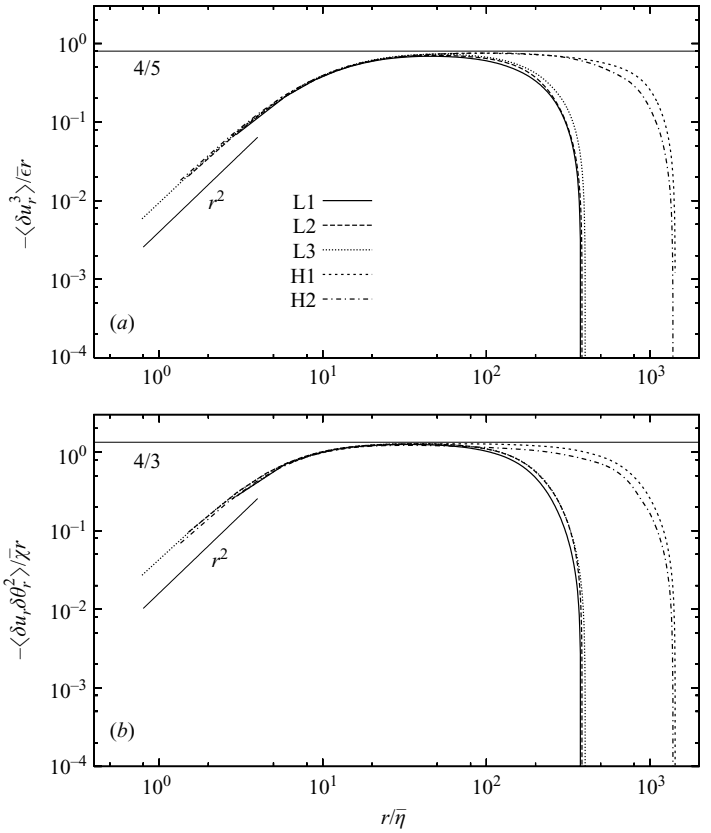

FIGURE 8. $K_{max}\overline{\eta}$ dependences of the approach of the curves to the (*a*) 4/5 law and (*b*) 4/3 law. The straight line represents the reference behaviour r^2 at the small scales expected from the structure function definition.

was due to the difference of the length of averaging time among them. The results described in this section suggest that low-order statistics in physical space are less sensitive to variations of $K_{max}\overline{\eta}$ than cases in wavenumber space.

3.4. *Effects on high-order structure functions*

As the order of the structure functions $S_q^{\alpha}(r)$ increases, the scaling in the ICR deviates from the KOC predictions and the intermittency becomes more noticeable (e.g. Warhaft 2000; Watanabe & Gotoh 2004). This also implies that the $K_{max}\overline{\eta}$ dependences of the structure functions become more significant at higher orders.

Figure 9 shows the DNS results for (*a*) $\hat{S}_q^L$, (*b*) $\hat{S}_q^T$, (*c*) $\hat{S}_q^{\theta}$, and (*d*) $\hat{S}_q^{\theta L}$ for $q = 4$ and 8. The width of the scaling ranges for the series L runs was not as wide as that for the series H runs because $R_{\lambda} = 180$ was not sufficiently large for a clear ICR to prevail compared to the case when $R_{\lambda} = 420$ (Watanabe & Gotoh 2004). Over the range $r < 10\overline{\eta}$, the slope of the structure functions varied slightly for different $K_{max}\overline{\eta}$; the difference became more significant as q increased. Over the range $r > 10\overline{\eta}$, $\hat{S}_q^L$ and $\hat{S}_q^T$ appeared to be almost independent of $K_{max}\overline{\eta}$ up to $q = 8$ as long as R_{λ} remained constant. However, we observed differences in the amplitudes of $\hat{S}_q^{\theta}$ and $\hat{S}_q^{\theta L}$, even though their functional forms were similar, irrespective of $K_{max}\overline{\eta}$.

If we write the structure functions as $S_q^{\alpha}(r) = C_q^{\alpha} r^{\zeta_q^{\alpha}}$ over the scaling range $\overline{\eta} \ll r \ll L$, the above observations may be summarized as follows: (i) the effects of the Reynolds

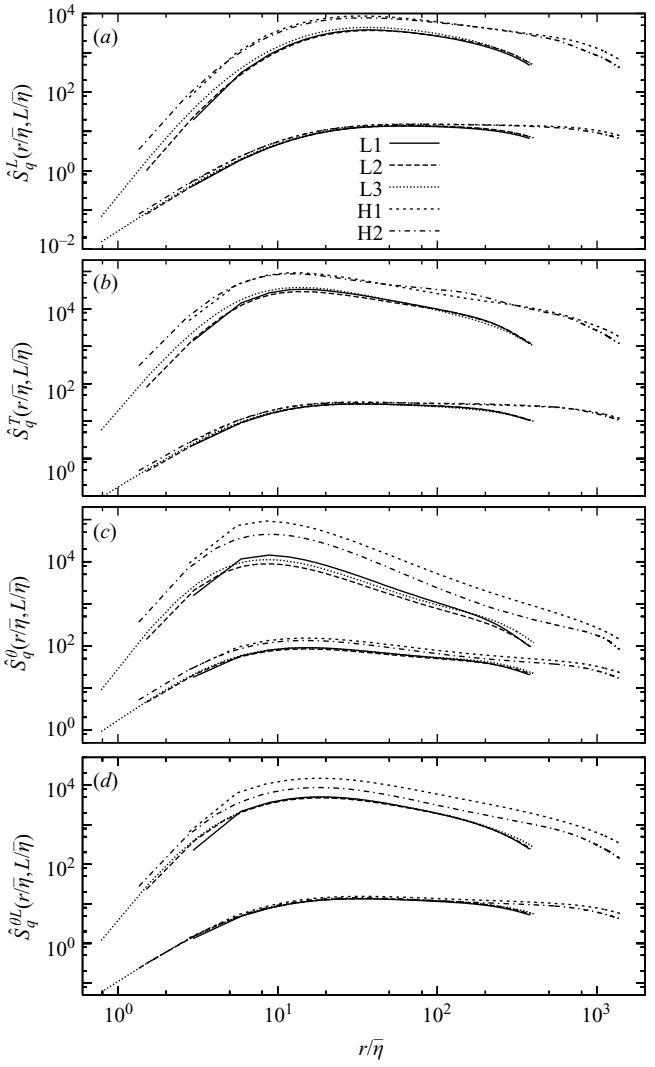

FIGURE 9. $K_{max}\overline{\eta}$ dependences of higher-order structure functions normalized by the KOC units (3.10) for (*a*) $\hat{S}_q^L$, (*b*) $\hat{S}_q^T$, (*c*) $\hat{S}_q^\theta$, and (*d*) $\hat{S}_q^{\theta L}$ with $q=4$ (lower curves) and $q=8$ (upper curves). The curves for $\hat{S}_8^\theta$ in (*c*) are multiplied by a factor of 0.02 to reduce the plotting range.

number and resolution appeared mostly in the prefactor C_q^α; (ii) these effects were less apparent on the slope of the curves; (iii) for a given order q, the prefactor increased with the Reynolds number; and (iv) the scatter of the prefactor due to variations in the resolution was more significant in the scalar and scalar flux than it was in the longitudinal and transverse velocity. Items (i)–(iii) indicate that the amplitudes (or prefactors) are Reynolds-number-dependent. Therefore, they are not universal for variations in large-scale conditions (Watanabe & Gotoh 2006*b*). The resolution dependence of the prefactors noted in item (iv) indicates a sensitivity to the dissipation scales. These facts imply that the rare-event statistics for scalar fluctuations are greatly affected by both the large- and small-scale conditions. The observed scatter of the prefactors for $S_q^\theta(r)$ and $S_q^{\theta L}(r)$ may be better explained by the

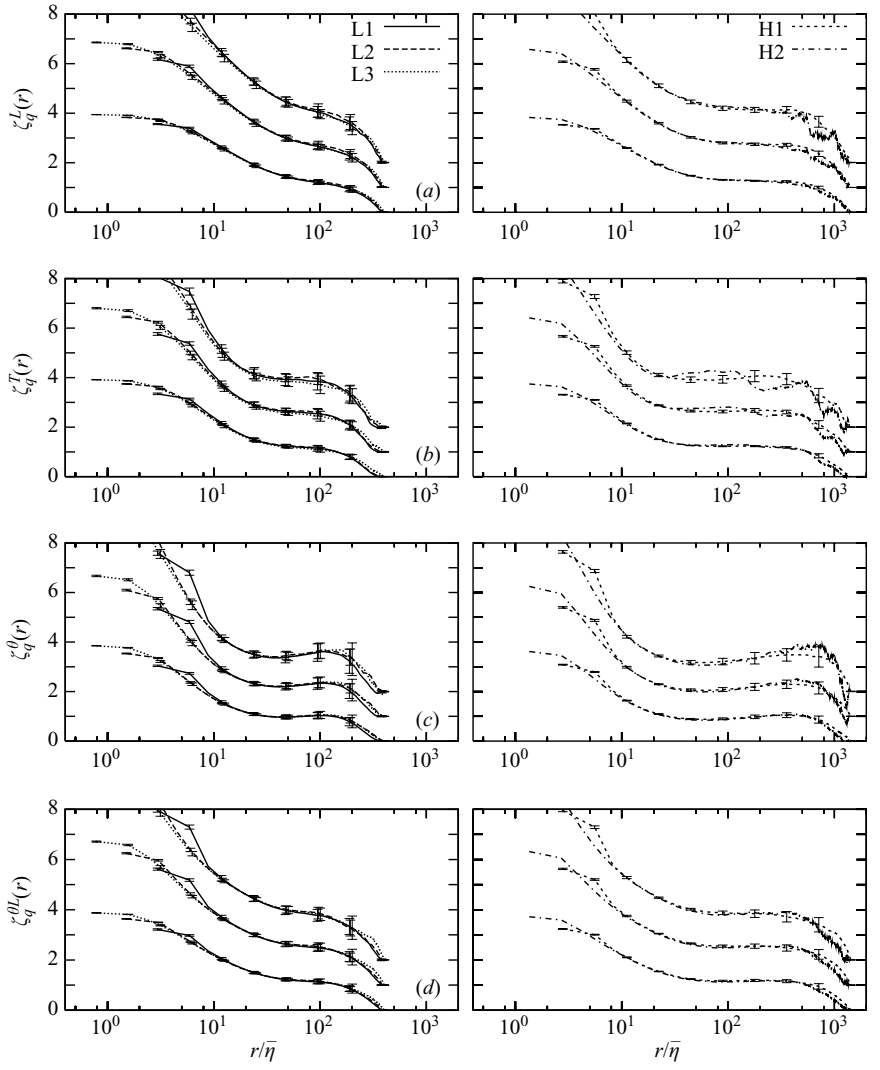

FIGURE 10. $K_{max}\overline{\eta}$ dependences of the local slopes for (*a*) $\zeta_q^L(r)$, (*b*) $\zeta_q^T(r)$, (*c*) $\zeta_q^\theta(r)$, and (*d*) $\zeta_q^{\theta L}(r)$. The curves in each figure correspond to $q = 4, 6$ and 8 from bottom to top. Error bars were estimated from the standard deviations of the temporal fluctuations in the quantities at each scales during the averaging time. The curves for $q = 6$ and 8 are shifted by adding a factor of 1 and 2, respectively, to their original values.

sensitivity of rare-event statistics to large-scale conditions, which are controlled by the duration of the temporal average, rather than their sensitivity to resolution effects. In the present study, the length of the temporal average decreased as the resolution increased, resulting in different large-scale conditions due to changes in the temporal average. Further examination is required using more reliable statistical data to draw a definite conclusion about the influence of the resolution on the prefactors.

The resolution effects on $S_q^\alpha(r)$ were investigated more carefully in terms of the scaling behaviour by examining their local slopes $\zeta_q^\alpha(r)$ defined by $\zeta_q^\alpha(r) \equiv \mathrm{d}\ln S_q^\alpha(r)/\mathrm{d}\ln r$. The variations in $\zeta_q^\alpha(r)$ with $r/\overline{\eta}$ for $q = 4, 6$ and 8 are shown in figure 10. The error bars were estimated from the standard deviations of temporal

fluctuations in the local slopes computed from the instantaneous velocity and scalar fields. The mean errors due to the temporal fluctuations increased with increase of the scale separation r, indicating a different convergence of statistics with respect to the variation in the scale r. The curves for run L3 confirm that the structure functions behave as $S_q^\alpha(r) \sim r^q$ over the range $r < \overline{\eta}$. This indicates that the velocity and scalar fields obtained by the DNS with $K_{max}\overline{\eta} \simeq 4$ (run L3) were adequately resolved and sufficiently smooth for scales less than $\overline{\eta}$. As expected, the curves for $r < 10\overline{\eta}$ were sensitive to $K_{max}\overline{\eta}$, which became more significant as q increased. However, the local slopes almost collapsed to a single curve, even at $q = 8$, over the range $r > 10\overline{\eta}$. The local scaling exponents over the range $10 < r/\overline{\eta} < 50$ obtained from the series L runs were very close to those obtained from the series H runs. These findings can be summarized as follows: (i) the local scaling exponents for $10\overline{\eta} < r \ll L$ converge to values different from those predicted by the KOC theory when the Reynolds number increases, and (ii) the dissipation intermittency does not affect the scaling behaviour of the structure functions over the scaling range of $r > 10\overline{\eta}$. These facts strongly suggest that local scaling exponents up to the eighth order over the range of $10 < r/\overline{\eta} < 50$ are independent of both the large and dissipation scales of motion, demonstrating the universality of the scaling exponents over the inertial range.

It is interesting to compare the scale $10\overline{\eta}$ to the characteristic scales of a vortex tube or cliff of the scalar field (Jimenez *et al.* 1993; Warhaft 2000). In turbulence, an intense vortex tube has a diameter of approximately 8–$10\overline{\eta}$ (Jimenez *et al.* 1993). The mean width of a cliff in low-temperature helium gas turbulence is $(13 \pm 3)\overline{\eta}$ for R_λ ranging from 100 to 650 (Moisy *et al.* 2001). These values are in good agreement with the scale $10\overline{\eta}$. Therefore, it is reasonable to assume that a DNS with $K_{max}\overline{\eta} = 1$ can accurately compute the local scaling exponents of the structure functions up to the eighth order for scales greater than $10\overline{\eta}$ as long as the Schmidt number is unity.

3.5. *Effects on the velocity and scalar-increment PDFs*

We examined the resolution effects on the behaviour of PDFs for the velocity and scalar increments. Figure 11 compares the normalized PDFs for (*a*) δu_r and (*b*) $\delta\theta_r$ at a separation distance r. Curves at a smaller separation distance correspond to PDFs with longer tails. The figure indicates that the asymptotic tails for δu_r tend to become wider as $K_{max}\overline{\eta}$ increases. The PDFs for δu_r became less sensitive to variations in $K_{max}\overline{\eta}$ and approached a normal distribution as the scale r increased. However, for a scalar increment, the asymptotic tails of the PDFs varied with the resolution, even at scales larger than $10\overline{\eta}$, although the PDF form for $r > 10\overline{\eta}$ around the most probable part was again insensitive to variations in $K_{max}\overline{\eta}$. This is demonstrated in figure 12. The form of the asymptotic tails of the PDFs was strongly related to large jumps in the scalar field, which were controlled by both large- and small-scale conditions; i.e. the structure of the cliffs in the scalar field were affected by small-scale conditions while the spatial distribution of the cliffs was influenced by the large scales of motion (Watanabe & Gotoh 2006*b*). Therefore, the possibility of a dependence of higher-order statistics at large scale on the dissipation-scale dynamics cannot be ruled out.

The behaviour of the PDF curves near the most probable part of figure 11 is plotted in figure 12 using linear scales. The weak intensity of fluctuations at scales smaller than $10\overline{\eta}$ changed with the resolution, especially for the scalar increment. The differences between curves at $r < 10\overline{\eta}$ (curves at $r = \mathscr{L}/256$ and $\mathscr{L}/128$) were more significant for $\delta\theta$ than for δu, as would be expected from figure 1(*d*). However, for separation distances larger than $10\overline{\eta}$, the results collapsed to almost the same

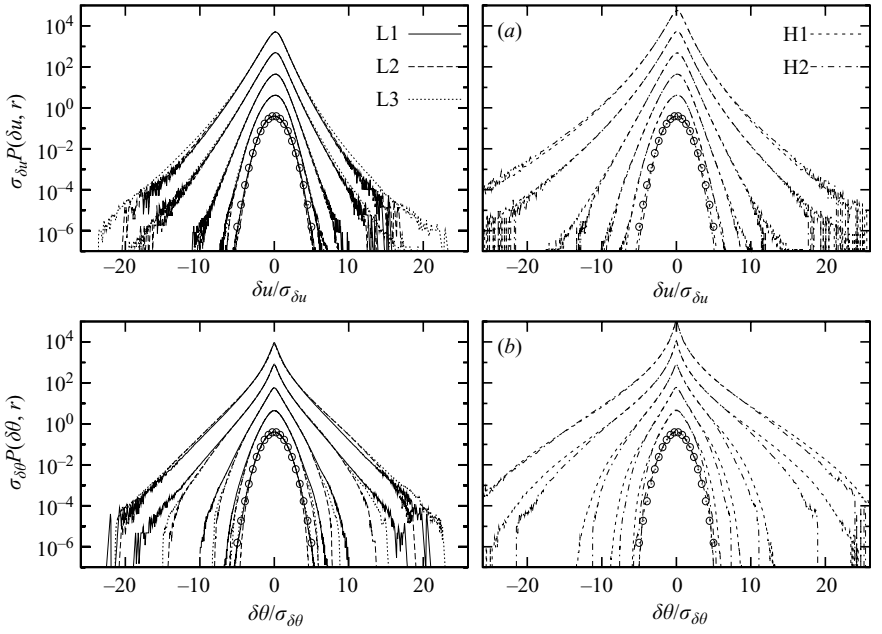

FIGURE 11. $K_{max}\overline{\eta}$ dependences of the normalized PDFs for the (a) longitudinal velocity increment (δu_r) and (b) scalar increment ($\delta\theta_r$). The curves are multiplied by a factor of 10^p ($p = 0, 1, 2, 3, 4$ (and 5 for the series H runs)) for $r = \mathscr{L}/2, \mathscr{L}/8, \mathscr{L}/32, \mathscr{L}/128, \mathscr{L}/256$ (and $\mathscr{L}/512$ for the series H runs) for clarity. The points $\circ$ denote the normal distribution. The scale $10\overline{\eta}$ is about $\mathscr{L}/80$ for the series L runs and $\mathscr{L}/290$ for the series H runs, respectively.

curve for both δu and $\delta\theta$. Thus, we conclude that the resolution effects for low-order statistics of the velocity and scalar increments when $q \leqslant 1$ are negligibly small for the scales of the ICR.

4. Discussion

4.1. *Resolution effects on derivative statistics in terms of multifractal theory*

We showed in § 3.1 that the resolution requirement for DNS is more stringent than the conventional condition $K_{max}\overline{\eta} = 1$ if we require accurate higher-order statistics of the derivative fields. The resolution effects are more significant for the asymptotic tail behaviour of PDFs for derivative fields such as $\partial_1 u_1$ and for dissipation fields. Therefore, the resolution effects are closely related to the details of the dissipation intermittency, as shown in the Appendix or Sreenivasan (2004). The PDF forms of the velocity gradient are reproduced in terms of the multifractal model of turbulence (Benzi *et al.* 1991), in which the asymptotic tail form of the PDF is controlled by the minimum value of a singularity exponent α_{min}. This suggests that the resolution effects on the statistics of the derivative field can be studied by regarding α_{min} as a cutoff filter that depends on the resolution.

The relationship between the resolution (Δx) and the strongest singularity may be given simply by (A 7) in the Appendix and the condition $\eta_{min} \approx \Delta x$:

$$N \equiv \frac{L}{\eta_{min}} \sim R_\lambda^{6/(\alpha_{min}+3)}. \tag{4.1}$$

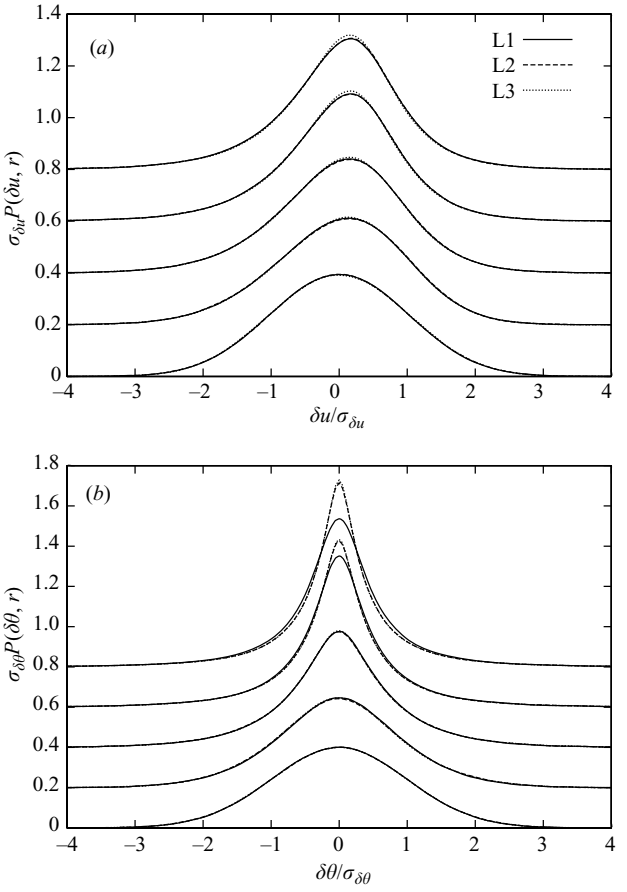

FIGURE 12. $K_{max}\overline{\eta}$ dependences of the normalized PDFs for the (a) longitudinal velocity increment (δu_r) and (b) scalar increment ($\delta\theta_r$), obtained from the series L runs. The curves in each figure correspond to $r = \mathscr{L}/2$, $\mathscr{L}/8$, $\mathscr{L}/32$, $\mathscr{L}/128$, and $\mathscr{L}/256$ from bottom to top, and are plotted by adding $0.2p$ ($p = 0, 1, 2, 3, 4$ in order) to the original values for clarity. Note that the curves from run L1 in (b) at $r \leqslant \mathscr{L}/128 \simeq 6\overline{\eta}$ deviate from those by the other runs.

Equation (4.1) suggests that α_{min} is a monotonically decreasing function of N, i.e. $\alpha_{min}(N) \sim (6 \ln R_\lambda / \ln N) - 3$ ($\geqslant 0$) when the Reynolds number R_λ is fixed. In this case, the resolution effects on fluctuations in energy dissipation can be represented using (4.1) and (A 9):

$$\frac{\epsilon}{\overline{\epsilon}} \sim N^{(3+\alpha_{min}(N))(1-\alpha)/(3+\alpha)}. \tag{4.2}$$

If we restrict our interest to the asymptotic tail behaviour of the PDF in $\epsilon/\overline{\epsilon}$, equation (4.2) can be reduced to the form $\epsilon/\overline{\epsilon} \sim N^{1-\alpha_{min}(N)}$ around $\epsilon \sim \epsilon_{max}$. The probability $Q(\alpha_{min})$ of finding α_{min} in the distribution of α in space is then simply evaluated by introducing the $f(\alpha)$ spectrum as $Q(\alpha_{min}) \sim N^{f(\alpha_{min})}/N^3 = N^{-3+f(\alpha_{min})}$. This leads to the N-dependence of the asymptotic tail behaviour of $P(\epsilon')$ for $\epsilon' = \epsilon/\overline{\epsilon}$:

$$\epsilon' P(\epsilon') = (\log N)^{-1} N^{-3+f(\alpha_{min})} h(\epsilon'/N^{1-\alpha_{min}}) \tag{4.3}$$

for the range $\epsilon \sim \epsilon_{max}$, where $h(x)$ is a non-dimensional scaling function. A possible minimum value of α_{min} inferred from experimental and DNS data is $\alpha_{min} = 0$ (Benzi

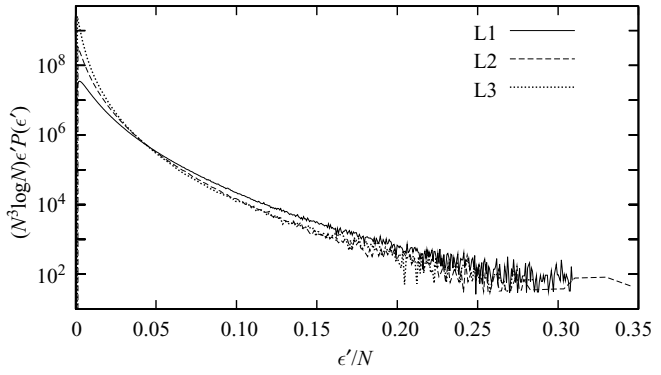

FIGURE 13. Scaling plot of the PDFs of the normalized kinetic energy dissipation $\epsilon' = \epsilon/\overline{\epsilon}$ obtained from the series L runs in terms of the resolution N.

et al. 1991). The geometry of the support for the spatial distribution of α_{min} is a point at which the maximum value of ϵ occurs; i.e. we approximately evaluate $f(\alpha_{min}) \simeq 0$. Figure 13 shows the scaling plot (4.3) with $\alpha_{min} = f(\alpha_{min}) = 0$ obtained using data from figure 3(*a*). The collapse of the curves in the asymptotic tail region is satisfactory, especially for runs L2 and L3. More details regarding the determination of PDF forms can be obtained by applying several multifractal models for $f(\alpha)$ spectrum (Benzi *et al.* 1991; Frisch 1995).

4.2. *Resolution effects on turbulence dynamics*

It is interesting to examine the resolution effects on the dynamics of turbulence and passive-scalar turbulence. To obtain an insight into the degree of the changes in the flow dynamics due to a finite resolution, it is useful to compare statistics from a coarse-grained turbulence field obtained by filtering an original field computed using the finest-resolution DNS with the statistics from a low-resolution DNS without filtering. For this purpose, it is convenient to introduce a cutoff wavenumber k_c in the Fourier space such that the coefficients of the Fourier series expansion of the velocity and scalar fields are decomposed into two components having smaller or larger wavenumbers than k_c as follows:

$$u_i(\boldsymbol{k}, t) = u_i^<(\boldsymbol{k}, t) + u_i^>(\boldsymbol{k}, t) = \mathscr{F} u_i(\boldsymbol{k}, t) + (1 - \mathscr{F}) u_i(\boldsymbol{k}, t), \tag{4.4}$$

$$\theta(\boldsymbol{k}, t) = \theta^<(\boldsymbol{k}, t) + \theta^>(\boldsymbol{k}, t) = \mathscr{F}\theta(\boldsymbol{k}, t) + (1 - \mathscr{F})\theta(\boldsymbol{k}, t), \tag{4.5}$$

where the spectral filter function $\mathscr{F}$ is defined using the Heaviside function $H(x)$ as $\mathscr{F}(k) = H(k_c - k)$. Hereafter the time argument is omitted for brevity. The scales of motion with $k < k_c$ are the grid scale (GS) and those with $k > k_c$ are the subgrid scale (SGS), following large-eddy simulation (LES) terminology (Pope 2000). In a typical LES, k_c is located midway in the inertial range, but we consider the case with k_c located in the dissipation range.

The equations of motion for the GS components $u_i^<$ and $\theta^<$ are

$$(\partial_t + \nu k^2) u_i^<(\boldsymbol{k}) = N_i^<(\boldsymbol{k}) + R_i^<(\boldsymbol{k}), \tag{4.6}$$

$$(\partial_t + \kappa k^2)\theta^<(\boldsymbol{k}) = N_\theta^<(\boldsymbol{k}) + R_\theta^<(\boldsymbol{k}), \tag{4.7}$$

where the first term on the right-hand side of (4.6) and (4.7) is the filtered nonlinear term composed from the GS components, which are defined by

$$N_i^<(\boldsymbol{k}) = \mathscr{F} M_{iab}(\boldsymbol{k}) \sum_{\boldsymbol{p},\boldsymbol{q}} u_a^<(\boldsymbol{p}) u_b^<(\boldsymbol{q}) \delta_{\boldsymbol{k},\boldsymbol{p}+\boldsymbol{q}}, \tag{4.8}$$

$$N_\theta^<(\boldsymbol{k}) = \mathscr{F}(ik_a) \sum_{\boldsymbol{p},\boldsymbol{q}} u_a^<(\boldsymbol{p}) \theta^<(\boldsymbol{q}) \delta_{\boldsymbol{k},\boldsymbol{p}+\boldsymbol{q}}, \tag{4.9}$$

with $M_{iab}(\boldsymbol{k}) \equiv (i/2)(k_a P_{ib}(\boldsymbol{k}) + k_b P_{ia}(\boldsymbol{k}))$ and $P_{ia}(\boldsymbol{k}) \equiv \delta_{ia} - k_i k_a / k^2$. $R_i^<$ and $R_\theta^<$ are the residual terms defined by $R_i^<(\boldsymbol{k}) = \mathscr{F}(\mathrm{N}_i(\boldsymbol{k}) - N_i^<(\boldsymbol{k}))$ and $R_\theta^<(\boldsymbol{k}) = \mathscr{F}(\mathrm{N}_\theta(\boldsymbol{k}) - N_\theta^<(\boldsymbol{k}))$, in which $\mathrm{N}_i(\boldsymbol{k})$ and $\mathrm{N}_\theta(\boldsymbol{k})$ represent the full nonlinear terms by $\mathrm{N}_i(\boldsymbol{k}) = M_{iab}(\boldsymbol{k}) \sum_{\boldsymbol{p},\boldsymbol{q}} u_a(\boldsymbol{p}) u_b(\boldsymbol{q}) \delta_{\boldsymbol{k},\boldsymbol{p}+\boldsymbol{q}}$ and $\mathrm{N}_\theta(\boldsymbol{k}) = ik_a \sum_{\boldsymbol{p},\boldsymbol{q}} u_a(\boldsymbol{p}) \theta(\boldsymbol{q}) \delta_{\boldsymbol{k},\boldsymbol{p}+\boldsymbol{q}}$. As shown by (4.6) and (4.7), the residual terms contribute to the GS dynamics from the SGS dynamics, representing the interaction between GS and SGS components of u_i and θ.

Let us locate the cutoff wavenumber in the range $1/\bar{\eta} < k_c < K_{max}$. Dropping the residual terms in equations (4.6) and (4.7) corresponds to the lower-resolution DNS with the largest wavenumber k_c without any SGS model. We want to examine how $R_i^<$ and $R_\theta^<$ affect the inertial- and dissipation-range statistics. To proceed with this analysis, we further integrated run L3 for a duration of $T = 1.4T_{av}$ and gathered two types of statistical data: those from the raw field with $k_c = K_{max}$ and data from the coarse-grained turbulence field with $k_c = K_{max}/4 > 1/\bar{\eta}$, which was generated from the same raw field.

Figure 14 compares the PDFs for the (*a*) longitudinal velocity gradient $\partial_1 \overline{u}_1$ and (*b*) scalar gradient $\partial_1 \overline{\theta}$ filtered with the different k_c in run L3. The probability of finding rare events decreased as the filtering scale increased. This trend is similar to the observation made from figure 1, which represents the decrease in intermittency with decrease of $K_{max}\bar{\eta}$. It is interesting to compare the curves from run L1 in figure 1 to those evaluated using $k_c = K_{max}/4$ in figure 14. This trend is also shown in figure 14. Both curves collapse to almost the same curve, although the curve for $\partial_1 \overline{u}_1$ deviates slightly from that obtained for run L1. This occurs because the curve of $k_c = K_{max}$ (bare field) in figure 14 is slightly different from that shown in figure 1 due to the difference of the length of averaging time between them. The flatness factor of $\partial_1 \overline{u}_1$ for $k_c = K_{max}$ in figure 14 is $F_L = 6.12$, which is less than the 6.61 given in table 2. We also examined how much F_L decreased in the lower-resolution DNS or for a larger filtering scale. The ratio of the flatness factor for run L1 to that of run L3 is 0.87 ($\partial_1 u_1$) and 0.70 ($\partial_1 \theta$) from table 2, which are comparable with the ratio of the flatness factor for $k_c = K_{max}$ to that for $k_c = K_{max}/4$, $5.62/6.12 = 0.92$ for $\partial_1 \overline{u}_1$ and $11.9/16.1 = 0.74$ for $\partial_1 \overline{\theta}$. These results indicate that the modifications to the dynamics induced by discarding the SGS components consisted of about 5% reduction in the flatness of the derivative fields. Most of this reduction may be attributable to the direct effects of filtering the raw fields. These results suggest that when $k_c\bar{\eta} > 1$, the effects of the residual terms arising from the SGS components are not significant in the turbulence dynamics responsible for the low-to-moderate-order statistics of the gradients of the velocity and scalar fields.

Figure 15 compares the square root of the spectra for the residual terms,

$$E_R(k \mid k_c) = 4\pi k^2 \langle |R_i^<(\boldsymbol{k})|^2 \rangle, \quad E_{R_\theta}(k \mid k_c) = 4\pi k^2 \langle |R_\theta^<(\boldsymbol{k})|^2 \rangle, \tag{4.10a,b}$$

and of the filtered nonlinear terms,

$$E_N(k \mid k_c) = 4\pi k^2 \langle |N_i^<(\boldsymbol{k})|^2 \rangle, \quad E_{N_\theta}(k \mid k_c) = 4\pi k^2 \langle |N_\theta^<(\boldsymbol{k})|^2 \rangle. \tag{4.11a,b}$$

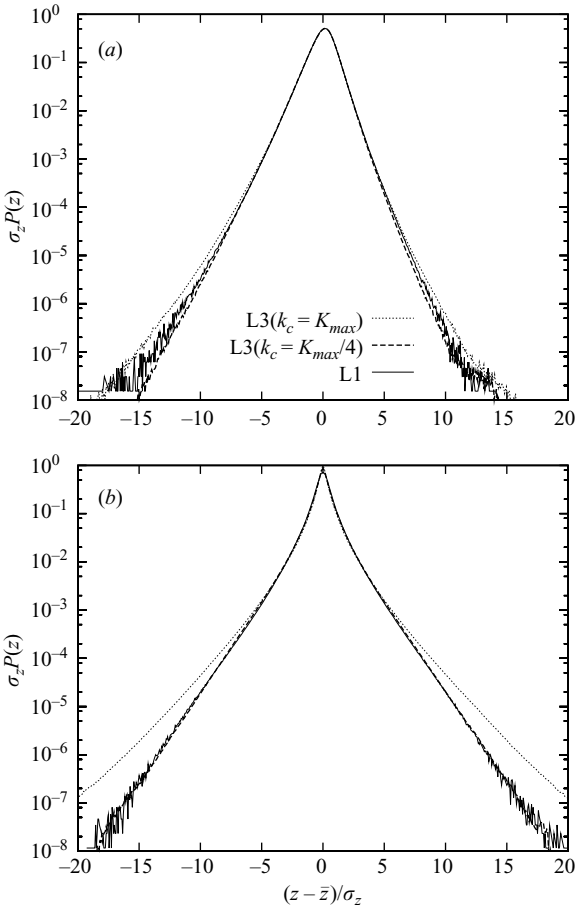

FIGURE 14. Comparison of the normalized PDFs for the (*a*) filtered velocity gradient $\partial_1 \overline{u}_1$ and (*b*) filtered scalar gradient $\partial_1 \overline{\theta}$ evaluated from the data of run L3. The cutoff wavenumber k_c is larger than the dissipation wavenumber $1/\overline{\eta}$ as $k_c = k_{max}/4$, which is comparable with the largest wavenumber in run L1.

The curves for $E_N(k\,|\,k_c)$ and $E_{N_\theta}(k\,|\,k_c)$ with $k_c = K_{max}/2$ and $K_{max}/4$ collapse almost perfectly on the curve of $k_c = K_{max}$ ($E_N(k)$ and $E_{N_\theta}(k)$). The spectra $E_R(k\,|\,k_c)$ and $E_{R_\theta}(k\,|\,k_c)$ grew sharply as k approached the cutoff wavenumber k_c and decayed as $E_R(k\,|\,k_c) \propto (k/k_c)^{3.2}$ and $E_{R_\theta}(k\,|\,k_c) \propto (k/k_c)^{3.0}$ when k moved to smaller wavenumbers. The sharp rise in the $E_R(k\,|\,k_c)$ and $E_{R_\theta}(k\,|\,k_c)$ is basically the same phenomenon found in the eddy viscosity near the cutoff, as discussed in previous spectral theory and DNS studies (Kraichnan 1976; Domaradzki & Rogallo 1990). For $k\overline{\eta} < 0.2$, the intensity of the residual terms in both the velocity and scalar fields were negligibly small compared to the filtered nonlinear terms $E_N(k\,|\,k_c)$ and $E_{N_\theta}(k\,|\,k_c)$, even when $k_c = K_{max}/4$, as expected. This fact strongly supports the conclusion in the previous section that the ICR statistics are insensitive to variations in the resolution provided $K_{max}\overline{\eta} \geqslant 1$.

4.3. *Implications of the resolution effects*

Several implications have arisen from our DNS turbulence resolution effects study.

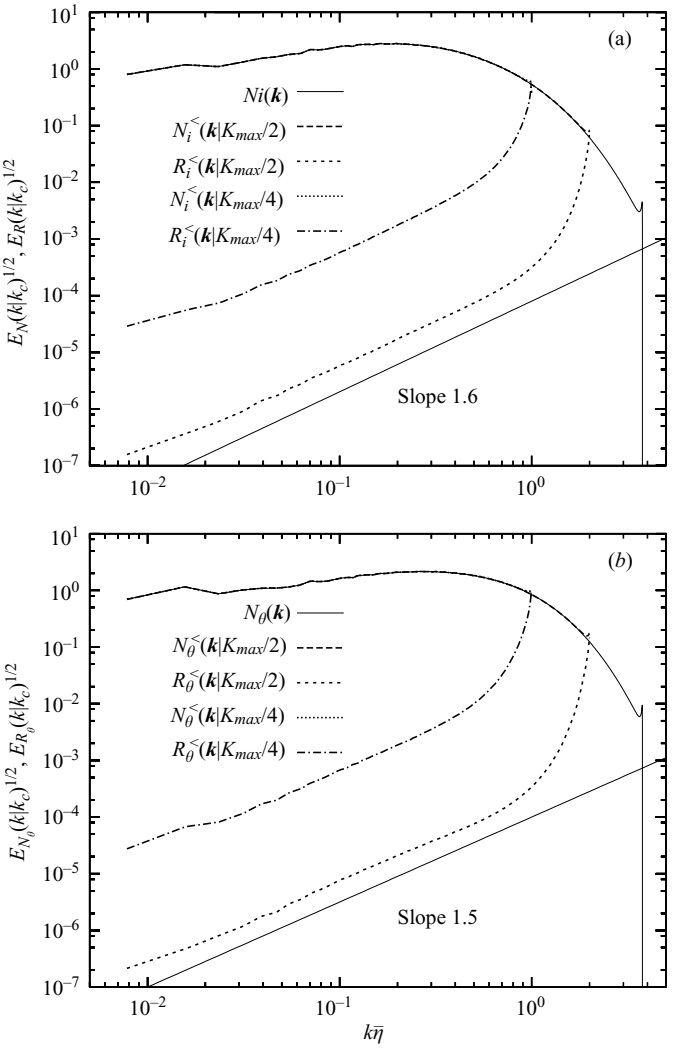

FIGURE 15. Square root of the spectra for the nonlinear and residual terms that appear in the equations of motion in terms of the filtered velocity and scalar fields for (a) velocity $N_i^<(\boldsymbol{k})$ and $R_i^<(\boldsymbol{k})$ and (b) scalar $N_\theta^<(\boldsymbol{k})$ and $R_\theta^<(\boldsymbol{k})$. The curves for $E_N(k\,|\,k_c)$ and $E_{N_\theta}(k\,|\,k_c)$ with $k_c = K_{max}/2$ and $K_{max}/4$ collapse almost perfectly on the curve of $k_c = K_{max}$ ($E_N(k)$ and $E_{N_\theta}(k)$).

First, knowing the resolution requirement to resolve the dissipation-scale eddies is useful when we consider the accuracy of experimental measurements of a turbulence signal or temperature fluctuations obtained using a probe, such as a hot wire. It is known that the degree of resolving fine-scale structures in the velocity and temperature fields depends strongly on the probe length l (Wyngaard 1968, 1971). If the probe length is longer than $\overline{\eta}$, any statistical quantities, such as the velocity gradients, are averaged over the probe length, which corresponds to the case of run L3 with $k_c < K_{max}$, as discussed above. Statistics with length scales greater than $10\overline{\eta}$ can be adequately obtained, for the low-to-moderate-order moments, corresponding to a probe length l of $l \leqslant \overline{\eta}$.

Second, the resolution problem in DNS can be considered from a universality viewpoint. So far, the universality of turbulence has been argued based on the

dependence of the small scales of motion on the large-scale conditions. However, in the classical sense of Kolmogorov (1941), a key fact is that the energy dissipation exists and is finite in the limit of zero viscosity, but the way the energy dissipates did not enter into the arguments because the theory is constructed on the grounds of a dimensional analysis, and no intermittency effects are taken into account. The inertial range is defined as the range over which the statistics are independent of both the large and dissipation scales of motion. However, in reality, intermittency exists and influences the scales in between the largest and smallest scales of motion. Changing k_c (or K_{max}) within the dissipation range can be interpreted as modifying the way for the energy to dissipate. The findings in the present study suggest that if most of the average dissipation rate is resolved in a DNS, the low-order statistics in the inertial range, especially the low-to-moderate-order local scaling exponents, are universal to variations in the dissipation.

5. Summary

We have examined the effects of variations in the dissipation-range resolution on the inertial- and inertial-convective-range statistics for turbulence and passive-scalar turbulence by performing DNS with several resolutions, where $K_{max}\overline{\eta} = 1$, 2, and 3.8 for $R_\lambda = 180$ and $K_{max}\overline{\eta} = 1$ and 2 for $R_\lambda = 420$. We discussed how variations in $K_{max}\overline{\eta}$ affected the behaviour of the fundamental statistics, such as the one-point PDFs for the velocity and scalar gradient fields, the kinetic energy and scalar variance spectra, the structure functions, and the PDFs for the velocity and scalar increments over scales ranging from $\overline{\eta}$ to L.

For one-point statistics, such as the gradients of the velocity and scalar fields, the second- and third-order moments were insensitive to variations in $K_{max}\overline{\eta}$. For high-order statistics of the derivative fields, the results obtained from a low-resolution DNS underestimated those from a high-resolution DNS. The contamination due to the poor resolution was significant for the high-order statistics of the gradient fields and for the statistics of the high-order derivatives.

Although the above-mentioned resolution effects on the fine-scale structure and derivative statistics have been examined with great attention in recent studies (Schumacher *et al.* 2005; Sreenivasan 2004; Yakhot & Sreenivasan 2005), further insight into the resolution problem of DNS was obtained by focusing on the effects of the dissipation-range resolution on the inertial-range statistics. For the low-order two-point statistics, such as the spectra and second-order structure functions, no significant $K_{max}\overline{\eta}$ dependences were observed over the entire scale range, except $k \sim K_{max}$ and $r > L$. Previously, the more stringent resolution requirement $K_{max}\overline{\eta} \simeq 1.4$ has been used to ensure the passive-scalar turbulence accuracy of a DNS, rather than imposing $K_{max}\overline{\eta} \simeq 1.0$ for the velocity only, even when $Sc = O(1)$ (Wang *et al.* 1999; Yeung *et al.* 2002; Sreenivasan 2004; Yeung *et al.* 2005). In the present results, however, no significant difference between a low-resolution DNS (runs L1 or H1) and a high-resolution DNS (runs L3 or H2) was detected for low-order statistics in the ICR. This fact encourages us to choose $K_{max}\overline{\eta} = 1$ when investigating the inertial-range statistics by performing a higher-resolution DNS to better understand the ultimate turbulent state, though it would be highly desirable to choose the more stringent resolution condition when the fine-scale dynamics in turbulence or in turbulence mixing has the greatest importance and significantly affects the dynamics over a wide range of scales.

The effects of the dissipation-range resolution on the inertial-range intermittency in the velocity and scalar fluctuations were also investigated by examining the behaviour of the high-order structure functions or the velocity and scalar-increment PDFs. The

accuracy strongly depended on $K_{max}\overline{\eta}$ over the range $r < 10\overline{\eta}$, but the structure functions, especially the scaling exponents up to $q = 8$, were little affected by $K_{max}\overline{\eta}$ when $r > 10\overline{\eta}$. As shown in figure 10, the local scaling exponents for the high-R_λ series of DNS had a finite plateau width in the scale range $r > 100\overline{\eta}$, irrespective of $K_{max}\overline{\eta}$. This suggests that the condition $K_{max}\overline{\eta} = 1$ is acceptable to ensure the accuracy of the scaling exponents of both the velocity and passive-scalar structure functions in the ICR.

The intermittency effects on the accuracy of the statistics can be viewed as the problem of the universality of the inertial-range statistics to changes of the dissipation range dynamics. When $K_{max}\overline{\eta}$ was approximately unity, the dissipation structure of the velocity and scalar fields was modified and differed from what would be obtained with an infinite resolution. This in turn indicates a modification to the means of the energy and scalar-variance dissipation. Therefore, the insensitive nature of the scaling exponents of the velocity and scalar-increment structure functions suggests an independence of the scaling exponents of the dissipation range, although the degree of independence depends on the order of the structure functions, the Reynolds number, and the Schmidt number.

In this paper, we showed that there was insufficient statistical data provided by run H2 which are constructed by a single snapshot. However this does not affect the main conclusion of the present paper regarding the low-order statistics. As for the structure functions at high order, it is desirable to obtain more converged statistical data to draw a definite conclusion from them. Moreover we examined only the case of $Sc = 1$. Since the resolution requirement of a DNS depends on Sc, it is necessary to examine the accuracy conditions for a passive-scalar DNS with $R_\lambda \gg 1$ and a general Sc case. Further computational resources are required to achieve $R_\lambda \gg 1$ and $Sc \gg 1$. Such a study is left for the future.

We thank the Earth Simulator Center, the Theory and Computer Simulation Centre of the National Institute for Fusion Science (NIFS05KTAT006), and the Information Technology Centre of Nagoya University for providing the computational resources. T. W. was supported by Grant-in-Aid for Scientific Research No.17760139 from the Ministry of Education, Culture, Sports, Science and Technology of Japan.

Appendix. Multifractal theory for energy dissipation intermittency

In this Appendix, we derive (1.4) by applying the multifractal theory of turbulence to the energy dissipation intermittency according to Sreenivasan (2004).

First we define the Reynolds numbers

$$R_L = \frac{u_{rms}L}{\nu}, \quad R_\lambda = \frac{u_{rms}\lambda}{\nu}, \tag{A 1a,b}$$

where $u_{rms} \sim (\overline{\epsilon}L)^{1/3}$. The definition of the mean Kolmogorov length (1.1) and (A 1a,b) yields the well-known relationship

$$\frac{L}{\overline{\eta}} \sim R_L^{3/4} \sim R_\lambda^{3/2}, \tag{A 2}$$

where we use $R_L \sim R_\lambda^2$ and $\lambda/L \sim R_L^{-1/2}$. If we regard $(L/\overline{\eta})^3$ as the degrees of freedom N^3 for the numerical turbulent motions, the relationship

$$R_\lambda \sim N^{2/3} \tag{A 3}$$

is obtained from (A 2). Equation (A 3) estimates the order of R_λ obtained by DNS with N^3 spatial grid points.

The energy dissipation rate locally averaged over the sphere $V_r = 4\pi r^3/3$ at the centre $\boldsymbol{x}$ is given by

$$\epsilon_r(\boldsymbol{x}) = \frac{1}{V_r}\int_{V_r} \epsilon(\boldsymbol{x}-\boldsymbol{x}')\,\mathrm{d}\boldsymbol{x}'. \tag{A 4}$$

The quantity ϵ_r plays an important role in the phenomenological cascade theory of turbulence via the refined similarity hypothesis proposed by Kolmogorov (1962), in which the statistics of the velocity increment are determined by those of ϵ_r with $R_\lambda \gg 1$. We define the local Reynolds number R_r at scale r as

$$R_r = \frac{\epsilon_r^{1/3} r^{4/3}}{\nu}. \tag{A 5}$$

The statistical self-similarity based on the multifractal theory of turbulence or the large-deviation theory (see Frisch 1995; Watanabe, Nakayama & Fujisaka 2000) suggests that ϵ_r is represented by the scaling form

$$\epsilon_r \sim \epsilon_L \left(\frac{r}{L}\right)^{\alpha-1}, \tag{A 6}$$

where $\epsilon_L = \overline{\epsilon}$ from the stationary condition of the system. The exponent α is the singularity exponent. The statistics of ϵ_r for $\overline{\eta} \ll r \ll L$ are characterized by those of the exponent α. Here we use the relationship (A 6) to the extent that (A 6) is satisfied at scales up to $r \sim \overline{\eta}$.

We define the fluctuating small scale η, where the nonlinear energy transfer balances with the kinetic energy dissipation, i.e. $R_r \sim 1$ for $r = \eta$. The scale η is the local Kolmogorov scale and fluctuates in space and time. We also set $\epsilon_\eta \simeq \epsilon$ because the spatial variation of ϵ is adequately smooth for $r \sim \overline{\eta}$, where the maximum of η is the order of $\overline{\eta}$. Then (A 5) and (A 6) yield

$$\frac{L}{\eta} \sim R_\lambda^{6/(\alpha+3)}. \tag{A 7}$$

This form can be rewritten by using (A 2) as

$$\frac{\eta}{\overline{\eta}} \sim R_\lambda^{-3(1-\alpha)/[2(3+\alpha)]}. \tag{A 8}$$

Thus, we arrive at the form

$$\frac{\epsilon}{\overline{\epsilon}} \sim R_\lambda^{6(1-\alpha)/(3+\alpha)}, \tag{A 9}$$

where $\eta/\overline{\eta} \sim (\epsilon/\overline{\epsilon})^{-1/4}$. The expression $\eta \sim \nu^{3/4}\epsilon^{-1/4}$ is used to derive (A 9). In the Kolmogorov scaling, ϵ_r does not depend on r, i.e. $\alpha = 1$. Equation (A 9) leads to this case: $\epsilon \sim \overline{\epsilon}$ with $\alpha = 1$. The strongest intermittency of the dissipation fluctuations in turbulence gives $\alpha = \alpha_{min}$, where ϵ has a largest value of ϵ_{max}. The most stringent requirement is the case of $\alpha_{min} = 0$ (Sreenivasan 2004), which leads to

$$\frac{\epsilon_{max}}{\overline{\epsilon}} \sim R_\lambda^2. \tag{A 10}$$

This relationship implies that $\epsilon_{max}/\overline{\epsilon}$ increases in proportion to R_λ^2. In addition, (A 7) and (A 10) yield

$$R_\lambda \sim \left(\frac{L}{\eta_{min}}\right)^{1/2}. \tag{A 11}$$

If we need to resolve the scales up to $\eta_{min} (< \overline{\eta})$ using DNS, the spatial grid points N must be set using $N = L/\eta_{min}$ to ensure the accuracy of the computations. Equation

(A 11) then estimates the largest R_λ that can be obtained by DNS. Note that exponent 1/2 is less than the value for the non-intermittent case, 2/3 in (A 3).

The scalar-dissipation scale with $Sc \geqslant 1$ can be obtained in a similar manner. We define the local Batchelor scale η_B by

$$\eta_B = \left(\frac{\nu\kappa^2}{\epsilon}\right)^{1/4} = Sc^{-1/2}\eta. \tag{A 12}$$

The degrees of freedom $N_B = L/\eta_B$ are evaluated using (A 7) and (A 12):

$$N_B \sim \left(\frac{L}{\eta}\right)\left(\frac{\eta}{\eta_B}\right) \sim Sc^{1/2}R_\lambda^{6/(3+\alpha)}. \tag{A 13}$$

The prefactor $Sc^{1/2}$ in (A 13) indicates that a more stringent DNS condition than only velocity field is required to resolve the scalar field with $Sc \gg 1$. The relationship between the Taylor-microscale Peclét number P_λ defined by

$$P_\lambda = \frac{u_L\lambda}{\kappa} = ScR_\lambda \tag{A 14}$$

and N_B is given by

$$P_\lambda \sim Sc^{(9-\alpha)/12}N_B^{(3+\alpha)/6}. \tag{A 15}$$

Equation (A 15) estimates P_λ obtained using a DNS with a fixed Sc and N_B. When the energy-dissipation intermittency is negligible, i.e. $\alpha = 1$, we obtain $P_\lambda \sim Sc^{2/3}N_B^{2/3}$. In contrast, $P_\lambda \sim Sc^{3/4}N_B^{1/2}$ is the case with the most intermittent energy dissipation, which is obtained by substituting $\alpha = \alpha_{min} = 0$ into (A 15).

REFERENCES

Batchelor, G. K., Howells, I. D. & Townsend, A. A. 1959 Small scale variation of convected quantities like temperature in a turbulent fluid. The case of large conductivity. *J. Fluid Mech.* **5**, 134–139.

Benzi, R., Biferale, L., Paladin, G., Vulpiani, A. & Vergassola, M. 1991 Multifractality in the statistics of the velocity gradients in turbulence. *Phys. Rev. Lett.* **67**, 2299–2302.

Bogucki, D., Domaradzki, J. A. & Yeung, P. K. 1997 Direct numerical simulations of passive scalars with $Pr > 1$ advected by turbulent flow. *J. Fluid Mech.* **343**, 111–130.

Chen, S. & Cao, N. 1997 Anomalous scaling and structure instability in three-dimensional passive scalar turbulence. *Phys. Rev. Lett.* **78**, 3459–3462.

Chen, S., Doolen, G., Herring, J. R., Kraichnan, R. H., Orszag, S. A. & She, Z.-S. 1993 Far-dissipation range of turbulence. *Phys. Rev. Lett.* **70**, 3051–3054.

Corrsin, S. 1951 On the spectrum of isotropic temperature fluctuations in isotropic turbulence. *J. Appl. Phys.* **22**, 469–473.

Domaradzki, J. A. & Rogallo, R. S. 1990 Local energy transfer and nonlocal interactions in homogeneous, isotropic turbulence. *Phys. Fluids* A **2**, 413–426.

Frisch, U. 1995 *Turbulence*. Cambridge University Press.

Gotoh, T., Fukayama, D. & Nakano, T. 2002 Velocity field statistics in homogeneous steady turbulence obtained using a high-resolution direct numerical simulation. *Phys. Fluids* **14**, 1065–1081.

Goto, S. & Kida, S. 1999 Passive scalar spectrum in isotropic turbulence: prediction by the Lagrangian direct-interaction approximation. *Phys. Fluids* **11**, 1936–1952.

Gotoh, T., Nagaki, J. & Kaneda, Y. 2000 Passive scalar spectrum in the viscous-convective range in two-dimensional steady turbulence. *Phys. Fluids* **12**, 155–168.

Gotoh, T. & Watanabe, T. 2005 Statistics of transfer fluxes of the kinetic energy and scalar variance. *J. Turbulence* **6**, No. 33 (18 pages).

Ishihara, T., Kaneda, Y., Yokokawa, M., Itakura, K. & Uno, A. 2005 Energy spectrum in the near dissipation range of high resolution direct numerical simulation of turbulence. *J. Phys. Soc. Japan* **74**, 1464–1471.

Jimenez, J., Wray, A. A., Saffman, P. G. & Rogallo, R. S. 1993 The structure of intense vorticity in isotropic turbulence. *J. Fluid Mech.* **255**, 65–90.

Kaneda, Y., Ishihara, T., Yokokawa, M., Itakura, K. & Uno, A. 2003 Energy dissipation rate and energy spectrum in high resolution direct numerical simulations of turbulence in a periodic box. *Phys. Fluids* **15**, L21–L24.

Kerr, R. M. 1990 Velocity, scalar and transfer spectra in numerical turbulence. *J. Fluid Mech.* **211**, 309–332.

Kolmogorov, A. N. 1941 The local structure of turbulence in incompressible viscous fluid for very large Reynolds number. *C. R. Acad. Sci. URSS* **30**, 301–305.

Kolmogorov, A. N. 1962 A refinement of previous hypotheses concerning the local structure of turbulence in a viscous incompressible fluid at high Reynolds number. *J. Fluid Mech.* **13**, 82–85.

Kraichnan, R. H. 1967 Intermittency in the very small scales of turbulence. *Phys. Fluids* **10**, 2080–2082.

Kraichnan, R. H. 1968 Small-scale structure of a scalar field convected by turbulence. *Phys. Fluids* **11**, 945–953.

Kraichnan, R. H. 1976 Eddy viscosity in two and three dimensions. *J. Atmos. Sci.* **3**, 1521–1536.

Meneveau, C. & Sreenivasan, K. R. 1991 The multifractal nature of turbulent energy dissipation. *J. Fluid Mech.* **224**, 429–484.

Moisy, F., Willaime, H., Andersen, J. S. & Tabeling, P. 2001 Passive scalar intermittency in low temperature helium flows. *Phys. Rev. Lett.* **86**, 4827–4830.

Monin, A. S. & Yaglom, A. M. 1975 *Statistical Fluid Mechanics, Mechanics of Turbulence*, Vol. 2, MIT Press.

Mydlarski, L. & Warhaft, Z. 1998 Passive scalar statistics in high-Péclet-number grid turbulence. *J. Fluid Mech.* **358**, 135–175.

Obukhov, A. M. 1949 Structure of the temperature field in turbulent flows. *Isv. Geogr. Geophys. Ser.* **13**, 58–69.

Pope, S. B. 2000 *Turbulent Flows*. Cambridge University Press.

Schumacher, J., Sreenivasan, K. R. & Yeung, P. K. 2005 Very fine structures in scalar mixing. *J. Fluid Mech.* **531**, 113–122.

Shraiman, B. I. & Siggia, E. D. 2000 Scalar turbulence. *Nature* **405**, 639–646.

Sreenivasan, K. R. 1995 On the universality of the Kolmogorov constant. *Phys. Fluids* **7**, 2778–2784.

Sreenivasan, K. R. 1996 The passive scalar spectrum and the Obukhov-Corrsin constant. *Phys. Fluids* **8**, 189–196.

Sreenivasan, K. R. 2004 Possible effects of small-scale intermittency in turbulent reacting flows. *Flow Turb. Combust.* **72**, 115–141.

Tsuji, Y. 2004 Intermittency effect on energy spectrum in high-Reynolds number turbulence. *Phys. Fluids* **16**, L43–L46.

Wang, L.-P., Chen, S. & Brasseur, J. G. 1999 Examination of hypotheses in the Kolmogorov refined turbulence theory through high-resolution simulations. Part 2. Passive scalar field. *J. Fluid Mech.* **400**, 163–197.

Warhaft, Z. 2000 Passive scalars in turbulent flows. *Annu. Rev. Fluid Mech.* **32**, 203–240.

Watanabe, T. & Gotoh, T. 2004 Statistics of a passive scalar in homogeneous turbulence. *New J. Phys.* **6**, 40 (36 pages).

Watanabe, T. & Gotoh, T. 2006*a* Intermittency, field structure and accuracy of DNS in a passive scalar turbulence. In *Proc. IUTAM Symp. on Elementary Vortices and Coherent Structures: Significance in Turbulence Dynamics* (ed. S. Kida). Fluid Mechanics and Its Applications, vol. 79, pp. 171–176. Springer.

Watanabe, T. & Gotoh, T. 2006*b* Intermittency in passive scalar turbulence under the uniform mean scalar gradient. *Phys. Fluids* **18**, 058105 (4 pages).

Watanabe, T., Nakayama, Y. & Fujisaka, H. 2000 Large deviation statistics of the energy-flux fluctuation in the shell model of turbulence. *Phys. Rev.* E **61**, R1024–R1027.

Wyngaard, J. C. 1968 Measurements of small-scale turbulence structure with hot wires. *J. Sci. Instrum.* **1**, 1105–1108.

Wyngaard, J. C. 1971 Spatial resolution of a resistance wire temperature sensor. *Phys. Fluids* **14**, 2052–2054.

Yaglom, A. M. 1949 On the local structure of a temperature field in a turbulent flow. *Dokl. Akad. Nauk. SSSR* **69**, 743–746.

Yakhot, V. & Sreenivasan, K. R. 2005 Anomalous Scaling of Structure Functions and Dynamics Constraints on Turbulence Simulations. *J. Statist. Phys.* **121**, 823–841.

Yeung, P. K., Donzis, D. A. & Sreenivasan, K. R. 2005 High-Reynolds-number simulation of turbulent mixing. *Phys. Fluids* **17**, 081703 (4 pages).

Yeung, P. K., Xu, S. & Sreenivasan, K. R. 2002 Schmidt number effects on turbulent transport with uniform mean scalar gradient. *Phys. Fluids* **14**, 4178–4191.